CHALMERS
UNIVERSITY OF TECHNOLOGY

The Noise and Vibration Transfer Characteristics of the Steering Installation in a Volvo FH Truck

Master's Thesis in the Master's programme in Sound and Vibration

GUSTAV FORSBERG
TOR MÖLLER

Department of Civil and Environmental Engineering
Division of Applied Acoustics
CHALMERS UNIVERSITY OF TECHNOLOGY
Gothenburg, Sweden 2015
Master's Thesis 2015:10

MASTER'S THESIS 2015:10

The Noise and Vibration Transfer Characteristics of the Steering Installation in a Volvo FH Truck

Master's Thesis in the Master's Programme Sound and Vibration

GUSTAV FORSBERG
TOR MÖLLER

Department of Civil and Environmental Engineering
Division of Applied Acoustics
CHALMERS UNIVERSITY OF TECHNOLOGY
Gothenburg, Sweden 2015

The Noise and Vibration Transfer Characteristics of the Steering Installation in a Volvo FH Truck
Master's Thesis in the Master's programme in Sound and Vibration
GUSTAV FORSBERG, TOR MÖLLER

Examensarbete 2015:10/ Institutionen för bygg- och miljöteknik, Chalmers tekniska högskola 2015

Department of Civil and Environmental Engineering
Division of Applied Acoustics
CHALMERS UNIVERSITY OF TECHNOLOGY
SE-412 96 Göteborg
Sweden
Telephone +46 (0)31-772 1000
Reproservice/Department of Civil and Environmental Engineering
Göteborg, Sweden 2015

Abstract

This thesis investigates in-cab sound levels from the power steering in a Volvo FH truck. The sound is most prominent when turning the wheels while the truck is parked. Previous research carried out at Volvo has shown that the main source is the hydraulic servo pump. It also showed that the steering shaft vibrations are fully dominated by the first pump order, whereas the in-cab noise is dominated by the second and third pump orders. The aim was to identify the transfer characteristics of different steering shaft prototypes and to study the influence of the steering installation from the steering gear and towards the cab interior in terms of noise and vibration. The work also includes a number of case studies such as the possible influence of the clock spring and driver introduced damping.

Three different steering shafts and a steering gear has been tested in both freely suspended conditions and mounted in a previous field test Volvo FH timber truck. The steering shafts were excited with a shaker and the response measured in multiple positions, both as vibrations and radiated noise.

The results indicate that the steering shaft is the main transfer path and does influence the noise radiation by its modal behavior. The cab suspension was also found to be an important transfer path up to around 200 Hz. Controlling the vibrations on the steering shaft will thus take limited effect on the first pump order as the cab suspension transfer path cannot be neglected. Measurements of radiated noise point towards that the steering shaft itself is one of the main noise radiators in the mid-high frequency range.

It was found that the torsional velocity is dominating on the upper part of the shaft. The radial and axial velocities are however what correlate best to radiated noise inside the cab. The total velocity level on the shaft is not representative for noise radiation. The prototypes showed no significant deviation compared to the standard shaft in terms of radiated sound and it is therefore recommended to make countermeasures closer to the source to produce larger sound reduction. It is recommended to improve the design of the steering shaft's axial bearing to increase the vibrational decoupling.

Keywords: power steering noise, steering shaft, servo pump noise, modal analysis, pump whining noise

Preface

This thesis has been carried out in cooperation with Volvo GTT and the Division of Applied Acoustics at Chalmers University of Technology. All work has been carried out at the Noise and Vibration Laboratory at Volvo GTT, Göteborg. First of all we would like to honour the entire team at the Noise and Vibration Laboratory for their continuous support during our work. A special thanks to our supervisor Theresia Manns and the manager of the department Christina Keulemans for showing great dedication in the project, also to rig technician Calle Wiman for helping with rigging and all sorts of practical matters. Finally we would also like to acknowledge our supervisor Patrik Höstmad at Chalmers for taking time to share his experience when discussing various measurement techniques, interpretation of results and support in vibro-acoustic measurement theory.

Gustav Forsberg, Tor Möller, Göteborg, December 2015

Contents

List of Figures

List of Tables

Chapter 1

Introduction

1.1 Background

Volvo GTT would like to gain further knowledge within the area of in-cab whining noise associated with the power steering. Such noise would typically arise under high steering loads combined with relatively low background levels, for example when ranging or turning the wheels when parked. In these driving cases the engine is often kept close to idle which will also minimise the background level.

Comprehensive testing and measurements with different trucks and pumps and steering gears established that the vibrations in the steering shaft was dominated by the fundamental pump order whereas the energy ratio of the noise in the cabin was altered towards higher levels of the first and second harmonic. The sum of the fundamental (P1) and the two following overtones (P2, P3) is henceforth referred to as the pump whining noise.

1.2 Previous Research

The main focus of Volvo GTT's previous research regarding noise from the power steering has been towards the hydraulic power side of the steering installation. The servo pump fundamental noise was found to be a good match to what noise was picked up inside the cab. Extensive research focused on the pump and steering gear was carried out to gain better understanding of the source and transfer characteristics. A number of abatement measures to the hydraulic high pressure pipe connecting the servo pump to the steering gear, has also been tested and some conclusions have been drawn towards possible suppressive actions. One of the more promising measures taken was replacing the hydraulic pipe with one of smaller internal diameter [1, 2].

Little work has been done so far on the low force side of the steering installation i.e. the steering shaft, console and the steering wheel. Different steering shafts and prototypes have been tested but the transfer function of this subsystem and how it transforms the noise is still unknown. It has however been established that around 90% of the pump whining noise enters the cab via the steering shaft, as the in-cab levels was reduced by circa 10 dB with the removal of this particular transfer path, see [2, app. 5b]. In Table 1.1 one can see the order representations from [1, p. 7]. The different orders are in reference to the engine crank shaft and corresponds to a frequency span of about 160-1000 Hz. The tests made in earlier engineering reports from Volvo GTT shows promising results from two prototype shafts. Also, some initial tests were done in [2] but no evident conclusions could be drawn.

Table 1.1: Order representations for two different servo pumps.

VDP	
P1:	19.25
P2:	38.50
P3:	57.75

(a) 11 impeller VDP order representations in relation to crank shaft.

FDP	
P1:	17.50
P2:	35.00
P3:	52.50

(b) 10 impeller FDP order representations in relation to crank shaft..

1.3 Purpose

A more elaborate survey within the area was of interest for Volvo to further expand the knowledge of the different prototype steering shafts. The purpose of this thesis was to investigate how the steering shaft together with the steering column transfers vibrations from the steering gear in to the truck cab.

1.4 Scope and Limitations

- In the measurements on the freely suspended steering shafts, parts above and below the universal joints are considered as rigid masses since they are relatively stiff compared to the main body of the steering shaft.

- Due to the complex design of the steering column and the vast amount of transfer paths to the cab floor, walls and panels, the vibration measurements inside the truck cab will be limited to the steering shaft.

- The complete vehicle measurements are limited to a single vehicle equipped with the correct steering installation.
- The steering gear is included in the vehicle measurements under the sole purpose of keeping the system as intact as possible and its vibrational behaviour from changing. Other than that, the steering gear sleeve to which the steering shaft clamps to is considered as the source.
- The steering wheel itself is not subject to any vibration measurements. A position just below the steering wheel is used as a reference.

1.5 Clarification of the issue

A pump whining noise generated from the power steering has been experienced when ranging. Another option than altering the source characteristics is isolating the cab by abatement measures to the main transfer path, i.e. the steering shaft. As the overtones of the servo pump fundamental are more prominent in the cab relative to the vibration levels measured directly above the steering gear, the vibration to radiated noise behaviour needs to be further examined. There are a number of possible causes besides resonant behaviour in the steering shaft, where one being the radiation efficiency of the steering wheel and other radiating parts inside the cab, and another being how the damping introduced by the driver's interaction with the steering wheel affects the harmonics compared to the fundamental pump order. The question has also been raised to what extent steering wheel position affects the noise transfer path. Finally what the clock spring, a component designed to electrically connect the steering wheel to the column, does to the emitted noise has been a factor of uncertainty during previous tests [1].

1.6 Objective

The main objective of this thesis is to measure and analyse the transfer characteristics of the steering shafts in both free and mounted conditions.

Furthermore, three case studies will be conducted:

- How does the driver influence the radiation by holding on to the steering wheel?
- How does the adjustment of the steering column affect the in-cab noise?

- Does the clock spring affect the noise radiation?

Based on the analysis of the steering shaft and column transfer path, together with the three case studies, final conclusions will be forwarded to Volvo.

1.6.1 Secondary Objectives

While working with the complete installation, the secondary objectives are to

- Identify main radiators
- Detect possible design modifications in the way the column is mounted to the cab
- Identify any connections that could transfer vibrational energy to other radiators than the steering wheel and column

These results will also be included in the recommendations.

Achieving high quality mobility measurements in rotational direction offers a great challenge as there is a rather limited selection of dedicated equipment for torsional wave analysis. A common measurement technique is using a torsional laser vibrometer. Since this was not available, the true angular velocity can be acquired in other ways. One of them is by using multiple accelerometers at different angles around the cross section of the object. By comparing tangential velocity at different angles the angular velocity is separated from any motion in the radial plane. The option chosen during this work is to create torsional excitation via an eccentric radial force. See section 4.1

Chapter 2

System Components

The complete steering installation in the Volvo FH truck can be broken down in to three subsystems, each with a number of individual components. The one component in which all three systems interact is the steering gear. The high force side connects the wheel hubs to the pitman arm via a heavy-duty linkage and the low force side connects to the steering wheel through the steering shaft and column. The power side with the servo pump and transfer pipes assists the driver with power when necessary. As the vibrations are known to origin in the pump, parts of the power side will be discussed for better understanding of the source characteristics. Other than that this chapter is devoted to describing the individual components on the low force side of the steering installation. Figure 2.1 show a schematic of the system.

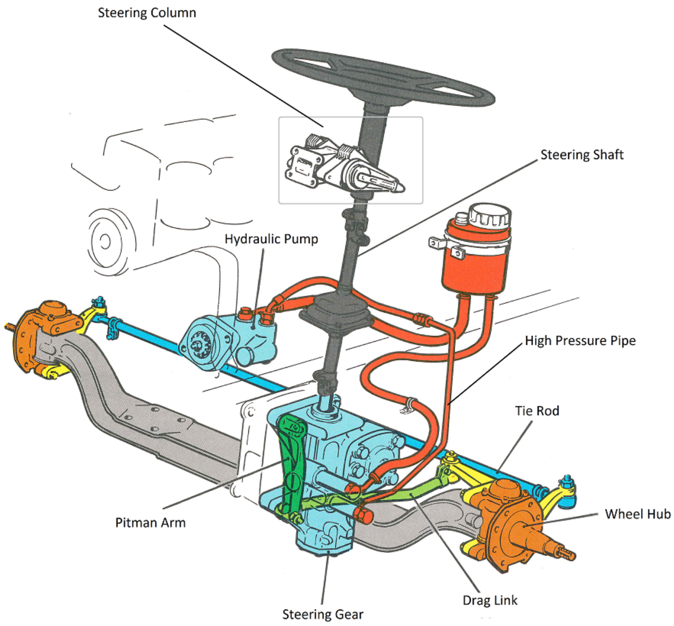

Figure 2.1: Schematic of the steering installation

2.1 The Steering Shaft

The steering shaft is designed as a flexible link transferring the motion from the steering wheel through the cab floor down to the steering gear, which is rigidly mounted to the frame. The shaft is equipped with universal joints in both ends to make it able to be mounted in an angle.

Since the truck cab is suspended from the frame, the steering shaft also contains a two part telescopic mechanism with a specially designed axial ball bearing, to make the shaft extensible in axial direction while keeping it rigid in tangential, or torsional, direction. This bearing itself has a travel of approximately 54 mm. The total travel is further extended to around 500 mm as the bearing, when out of travel, slides inside the cylinder part of the shaft. By allowing the bearing to act as a bushing it helps extending the shaft enough to allow for proper steering wheel positioning as well as tilting of the cab. The system is self adjusting to set the travel within the limits of the bearing while driving as this minimizes the transferred axial vibrations. The condition under which the telescopic mechanism operates within the range of the bearing will be referred to as the floating mode. Furthermore, the outer pipe will be referred to as the cylinder, and the inner solid rod as the piston. The parts of the steering shaft can be studied in Figure 2.2. Note that this is not an exact drawing of the standard shaft.

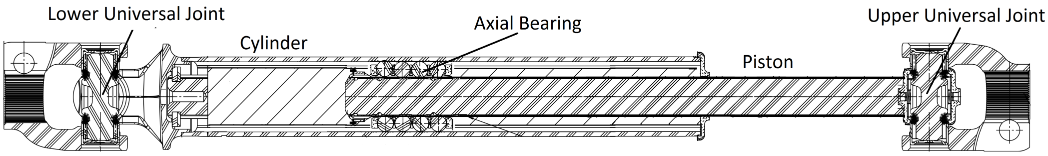

Figure 2.2: Components of the steering shaft

2.2 Prototype Steering Shafts

This section describes and show the different prototype shafts examined in this report. The prototypes has been handed to Volvo by the supplier for steering noise suppression testing. The basic design for the prototype are the same as for the productions shaft but with some added features. The shafts can be seen in Figure 2.3.

The NVH shaft is specially designed to reduce improving noise and vibration transfer. It has what the supplier calls a 'scraper design', an alternative scraper seal design between the cylinder and the piston.

The 834g shaft is essentially a standard shaft that has $2 * 417$g added mass to its lower end to improve noise and vibration transfer suppression.

Figure 2.3: The three different steering shafts from top to bottom: 834g, NVH and Standard.

2.3 The Steering Column

The steering column joins the steering wheel to the steering shaft. The design enables the driver to freely adjust the steering wheel to the preferred driving position, while acting as a rigid mount once the positioning is set. The steering wheel can also be moved out of the drivers way while entering or exiting the cab. The great versatility of the steering wheel positioning makes the steering column a rather complex component, and is shown in Figure 2.4.

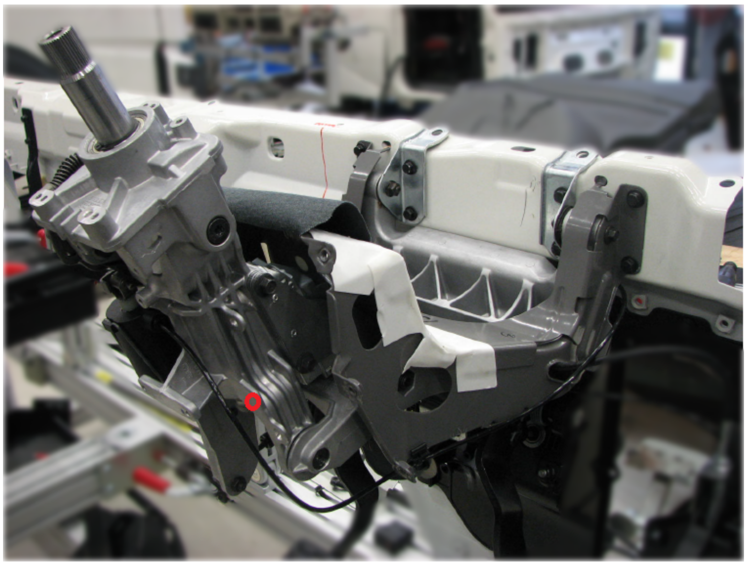

Figure 2.4: Steering column mounted to the firewall.

Horizontal control arms link the bottom of the column to the firewall, allowing vertical motion as well as motion in and out from the dashboard and firewall. The column is then held in place by a multiple disc locking mechanism operated via a two stage foot pedal. Besides the mechanical disc lock, the pedal also contains a pneumatic valve controlling the upper tilt mechanism called the neck tilt. This function allows the driver to adjust the angle of the steering wheel without dislocating the main position. The small pneumatic cylinder operates a spur locking mechanism making angle adjustments in discrete steps possible. The whole setup is mounted to the firewall via two rubber bushings at the top, the lower mount is a relatively stiff steel console.

2.4 The Power Steering

The power steering mainly consists of two parts. The steering gear and the hydraulic servo pump. The steering shaft is connected to the ball screw on top of the steering gear, which can be seen in the lower right corner of Figure 2.5. The bottom of the ball screw is connected to the working piston that via a splined axle, seen in the upper right corner of Figure 2.5, moves the pitman arm, and thus also the wheels.

To aid the driver by reducing the amount of force that has to be put in to the steering wheel, a rotary valve is set to allow the hydraulic oil from the servo pump to be pushed in, either above or below the working piston, depending on which way the steering wheel is turned. This construction makes it able to steer the vehicle even if the servo pump is not working.

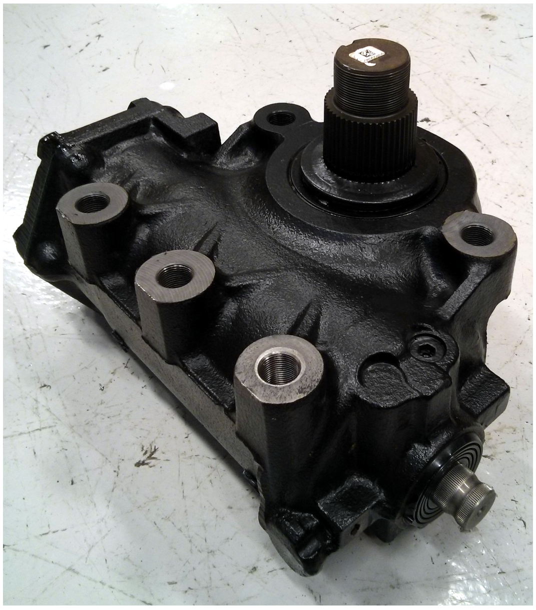

Figure 2.5: The steering gear

Chapter 3

Method

The following chapter contains a description of the main objectives during the work and the method and setup of achieving these goals. It also contains a detailed approach to conducting the measurements explained in this report and what equipment used to conduct the measurements.

3.1 Literature

An investigation has been carried out at Volvo GTT within the area of in-cab power steering noise. In [2], Kaj Bodlund showed that the servo pump was the system source and that the transfer characteristics to the cab has a direct connection to the orders of the servo pump.

3.2 Measurements

To gain better understanding of how the low force side of the steering installation influences the generated noise, a number of different measurements has been carried out. This section describes the measurement procedures as well as the system environment.

3.2.1 Freely Suspended Steering Shaft

The steering shaft was studied as an isolated object. This allows for analysis in resonant behavior and possible non-linearities caused by, for example, the universal joints or the telescope mechanism. Coupling between different wave-types are also investigated. The available prototype shafts are compared and their design changes evaluated. With the steering shaft freely suspended and excited with a shaker, its vibrational characteristics was measured with accelerometers. The shafts were excited in axial, radial and tangential directions in consecutive tests.

3.2.2 Complete In Vehicle Installation

By exciting the steering shaft just above the steering gear the fluid borne excitation from the servo pump can be simulated. Shaker excitation also means higher repeatability than by manually turning the steering wheel, as was done in earlier tests. With a powerful enough excitation, this method also covers the structure to airborne transition. This is proven to be helpful when subjectively identifying main radiators as the background levels are considerably lower without the engine running. The sound levels in the cab was measured during all trials and correlated to vibration levels along the steering shaft.

3.2.3 In Vehicle Case Study

Besides studying the transfer function of the complete system a number of cases was tested in this setup. The influence of steering wheel position to radiated sound is one parameter. Another how the damping introduced by a human holding on to the wheel affects the noise level. One case involves whether the clock spring has any influence to the vibrations transferred. The different prototypes was also tested and compared to the isolated tests. During the work with the complete assembly a secondary target was to identify any points of strong coupling between the steering column and the dashboard or cab shell. Paths that potentially could transfer energy to other radiators than the steering wheel and column.

3.2.4 Shaker Measurement

When conducting shaker measurements cautiousness of mass loading from the transducers must be taken. Generally a good rule of thumb is that the mass of the transducer should not be larger than 10% of the apparent mass in the measuring point. To avoid problems with mass loading, all transducers should be mounted at once to make sure that the measured structure is the same at all times. If the transducers are removed, dummy masses should be put in the same spot to keep the structure intact [3, p. 18].

3.3 Equipment

This section lists all the equipment used during measurements. It also states the placements of the accelerometers and other measurement and also how the rig was set up.

3.3.1 Software and Data Acquisition

Müller BBM PAK MkII is a mobile measurement system for acoustic and vibration measurements. It allows for both signal generation and up to 40 channels of data acquisition simultaneously. With the associated software running on a portable laptop, this system is applicable for both lab and on the field measurements [4].

3.3.2 Sensors and other hardware

All vibrational measurements was made with ICP type accelerometers. These accelerometers contains microelectronic that convert the high impedance signal from the piezoelectric element to a usable low impedance signal suitable for sending through cables. The PAK Mk II has built in constant current signal conditioners so that easy auto ranging from the different accelerometers can be set to make the signals sufficiently high.

The triaxial accelerometers were screwed to adhesive mounting bases that were glued to the shaft with quick bonding gel. This way of mounting, on a flat surface, has a sensitivity deviation at around 50 kHz, see curve 3 in Figure A.1 [5]. Since the shaft has a circular shape we can expect this deviation to occur at a lower frequency but not nearby the region of interest, which in this case has an upper limit of 1 kHz. The single axis accelerometers were mounted to a glass reinforced polycarbonate clip that was glued to the shaft. This clip lower the high frequency response somewhat but not enough to be relevant in this context.

A vibration exciter, also known as shaker, from Brüel & Kjær was used to excite the structure. This device features a force rating of 45 Newton sine peak, within the frequency range of 10-20,000 Hz. It was mounted to both a steel stand to make it able to excite structures along the horizontal plane and hung up in rubber cords for the in-vehicle measurements. [6].

Chapter 4

Setup

This chapter explain the details of the test setup and data acquisition.

4.1 Measurement theory

Exciting the structure while measuring the true input force is somewhat complicated when using traditional shakers and force transducers. The option chosen during this work is to create torsional excitation via an eccentric radial force. The disadvantage with this particular method is that the total input force will be split between torsional and radial excitation. This means that the exact input force cannot directly be measured since the input force is measured at the top of the mount and will consist of the two contributing directions, see Figure 4.4.
In order to distinguish between the torsional and radial forces, some backwards calculations from a previously measured radial mobility can theoretically be done as follows.

For harmonic motion, the mobility is generally defined as:

$$Y(\omega) = \frac{ve^{j\omega t}}{Fe^{j\omega t}} = \frac{v}{F}$$

Where v is velocity, F is force, j is the imaginary unit, ω is the angular frequency and t is time.

Since we can measure the velocity with an accelerometer, and the input force with a force transducer, the input mobility for the radial measurement is easily obtained:

$$Y_r = \frac{v_r}{F_r}$$

Where v_r is the radial velocity and F_r is the force in radial direction.

We know that the total measured force in the driving point for the torsional measurement is

$$F_{tot} = F_r + F_t$$

Where F_t is the force in torsional direction.

The torsional mobility can thus be calculated by taking

$$Y_t = \frac{v_t}{F_t} = \frac{v_t}{F_{tot} - F_r} = \frac{v_t}{F_{tot} - \frac{v_r}{Y_r}}$$

Using this type of inverse method is however prone to generate large errors were Y_r is small, for example in anti-resonances. There are better ways and other types of algorithms that would produce a more accurate estimation, such as an LMS-algorithm.

After a set of initial measurements, the decision was made to base the mobility on the total measured force. This because of higher relative levels in secondary directions when exciting in radial direction than in torsional, thus rendering the purpose of the approach inapplicable.

It was also decided to base the torsional mobility calculations on tangential velocity over force instead of angular velocity over torque. This compromise makes comparison to other wave types and directions easier and means no loss of information as the transformation is simply an offset in the decibel scale.

In this particular setup the true torsional mobility, Y_t $[\frac{rad*s^{-1}}{Nm}]$ is obtained by adding an additional 53.3 dB as $r_{exc} = 0.080\ m$ and $r_{sensor} = 0.027\ m$. The transformation factor is found as $20 * Log_{10}(\frac{1}{r_{exc}*r_{sensor}})$ going from $[\frac{m*s^{-1}}{N}]$ to $[\frac{rad*s^{-1}}{Nm}]$.

4.2 The Freely Suspended Steering shaft

The steering shaft under study is hung in springs from a steel structure and excited with a shaker placed on the floor. Suspension resonances is estimated to around 2-3 Hz. In tangential configuration a second order resonance is found at 20 HZ.

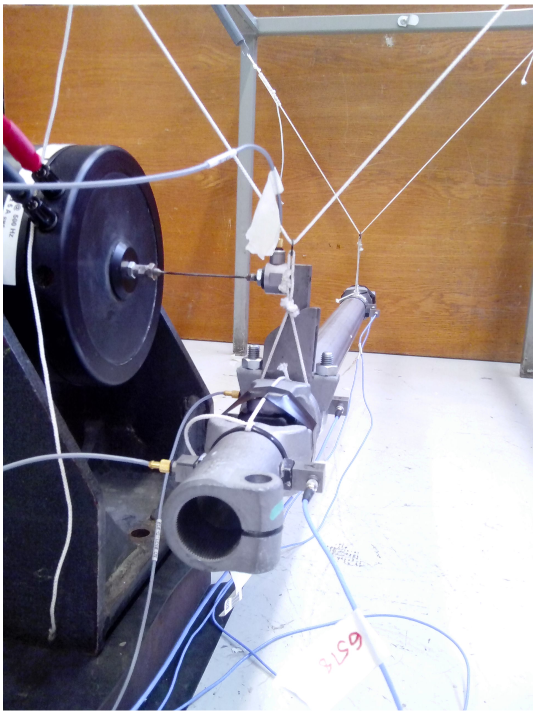

Figure 4.1: Setup for excitation in tangential direction.

During normal operation the telescopic extension of the steering shaft ranges from 60 mm–300 mm, depending on the configuration of the truck and the position of the steering wheel. The response was consequently measured with 60 mm, 200 mm and 300 mm extension of the telescope, all in floating mode. The shafts were excited in axial, radial and tangential direction in consecutive measurements. The output signal is set to bandpass filtered white noise, ranging from 10 Hz to 5000 Hz throughout the trials. Frequency resolution is set to 1 Hz via a block size of 32768, sampling rate 32768 Hz with a Hanning window. Each measurement is averaged 25 times with no overlap.

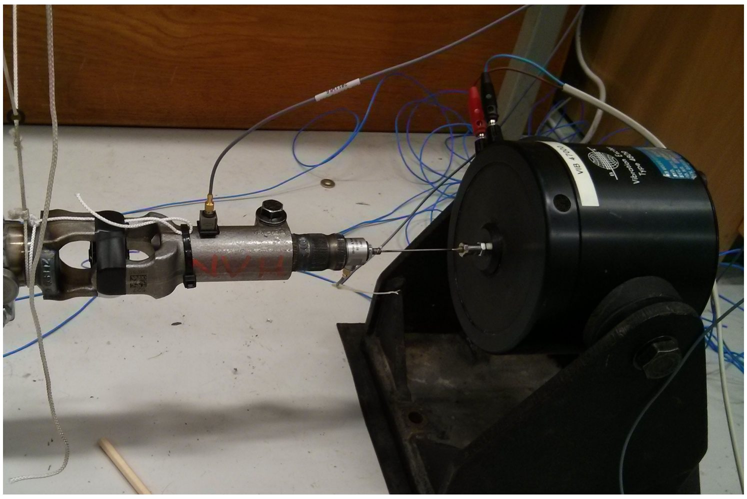

Figure 4.2: Setup for excitation in axial direction.

In order to prevent the lower half of the universal joint from moving, it was secured with a string and electrical tape.

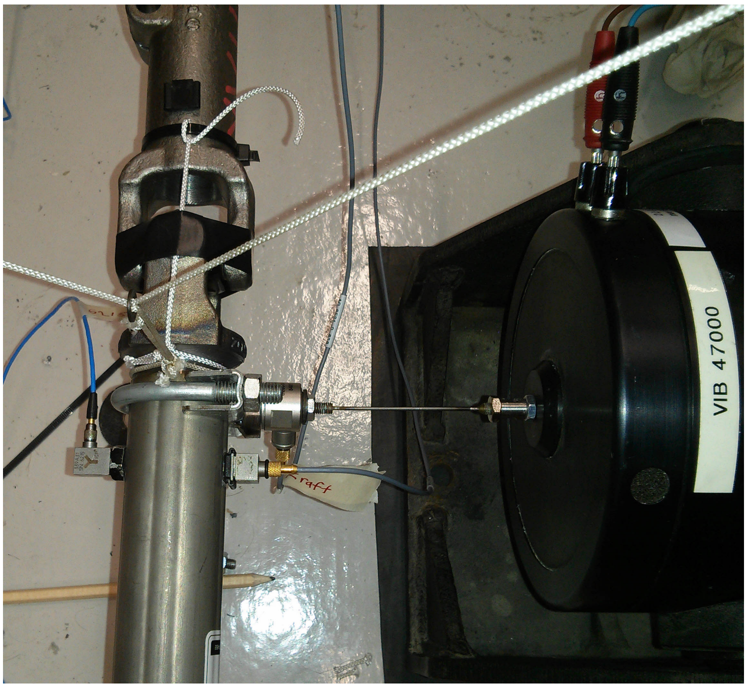

Figure 4.3: Setup for excitation in radial direction.

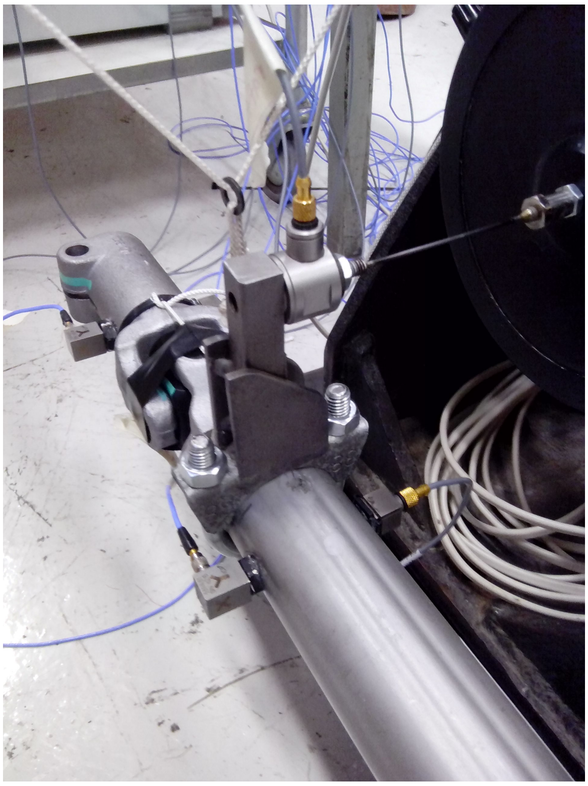
Figure 4.4: Setup for excitation in tangential direction.

In this setup a complementary single axis accelerometer is placed on the opposite side of the triaxial accelerometer in order to differentiate torsional motion from radial motion.

Chapter 5

Analysis

5.1 Standard Shaft

This section contains a detailed analysis of the standard shaft, using measured mobilities and Matlab models and visualisations. Most of the results presented in this section is also applicable to the other prototypes tested. The directions stated in subsection 5.1.1 to subsection 5.1.3 refers to the direction of both excitation and measured response.

5.1.1 Axial Direction

With the shaft freely suspended and excited in axial direction the response is very similar to that of two mass-spring systems in series, as seen in Figure 5.2. In this measurement, position 15 corresponds to the input mobility and position 1-4 are transfer mobilities, as seen in Figure 5.1.

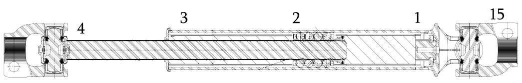

Figure 5.1: Measurement positions during axial measurements.

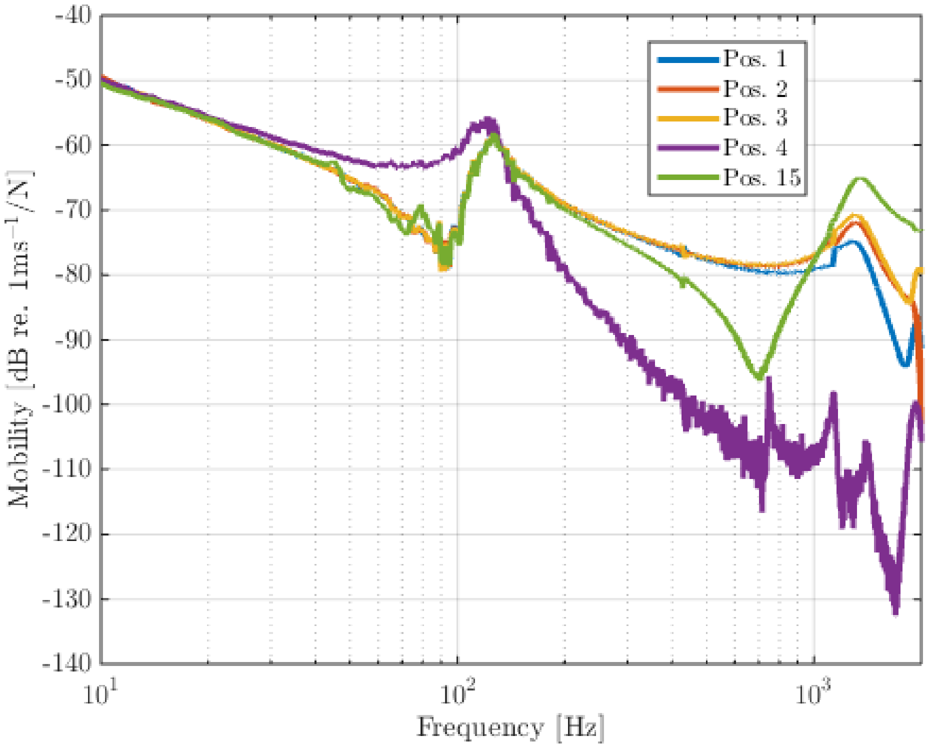

Figure 5.2: Measured axial mobility for standard shaft excited in axial direction with 300 mm extension.

The first resonance around 120 Hz origins from how the telescope mechanism couples the two main part of the shaft together and strongly depends on the design of the telescope bearing. A lower resonance frequency was expected since the bearing rolls with little friction, within the floating mode, when operated manually. A quick test measurement show that when not in floating mode this particular resonance is increased approximately 50 Hz in frequency. The bearing seems to handle torque rather well, but the torque applied during steering might slightly increase the resonance frequency. During the measurements the bearing was found to be very sensitive to bending forces, as even a small force increased the friction a lot. This behavior was however experienced when manually handling the shafts and has not been measured. Similar sensitivity to bending forces was also subjectively experienced during the in-vehicle measurements. The latter resonance around 1300 Hz is due to the lower universal joint and can be further studied in Figure 5.4.

In axial direction the three different telescope extensions tested produce similar results. The 200 mm extension shows higher damping in the 100 Hz region, a possible explanation is the damping connected to this resonance depends on the ratio of the air volumes behind and in front of the bearing. The behaviour has however not been further studied. Figure 5.3a shows transfer mobility across the universal joint, Position 1. Figure 5.3b shows transfer mobility to the far end, Position 4.

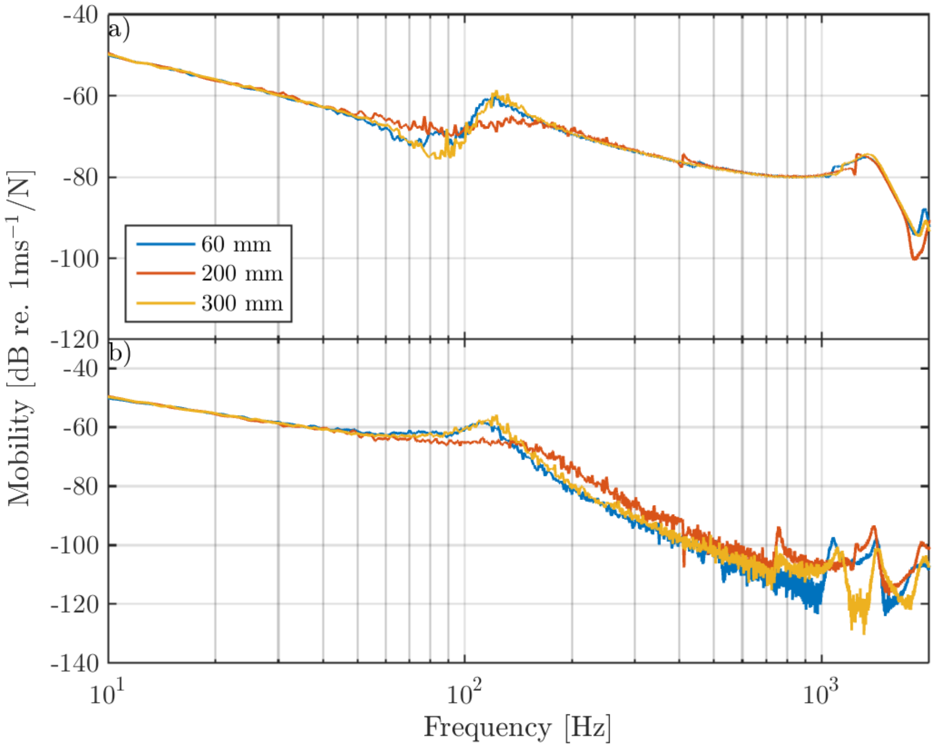

Figure 5.3: Measured axial input mobility a), and transfer mobility b), in axial direction for three different telescope extensions.

The behavior of the lower universal joint was studied separately in the directions deemed possible under free conditions, i.e. axial and tangential direction. For radial direction, see subsection 5.1.5. The joint behaves much like a mass-spring system and the resonances are clearly visible in Figure 5.4 and Figure 5.5. With the shaft mounted these resonances are expected to appear lower in frequency due to added mass from the steering gear. The upper joint should produce similar response. The measured response is likely slightly more damped than it would have been without the tape used to stabilize the universal joint during measurements.

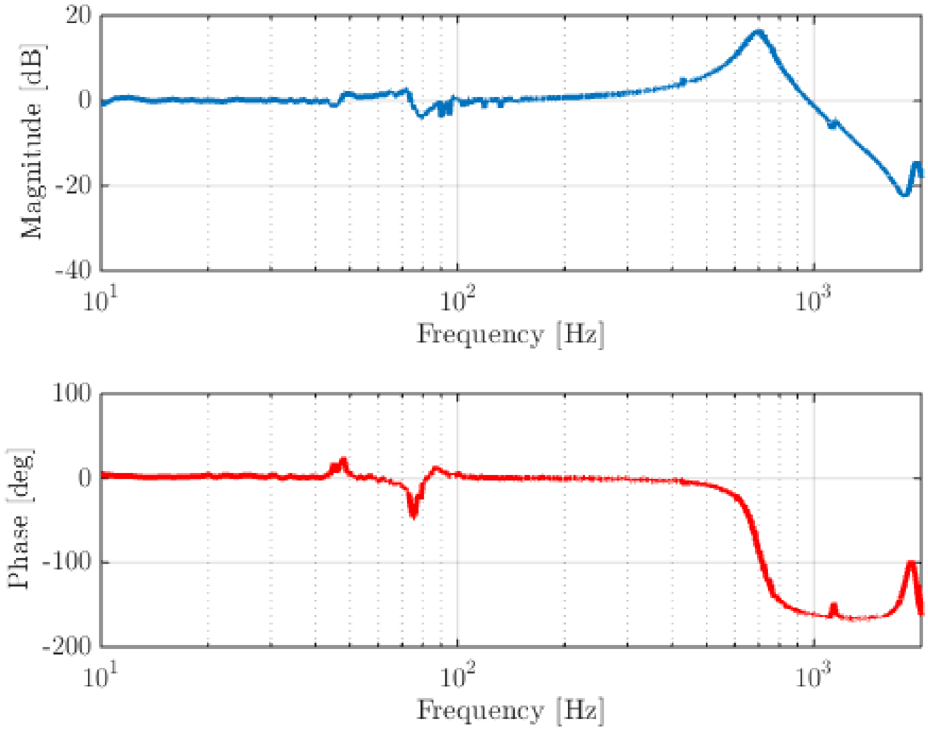

Figure 5.4: Transfer Function for universal joint in axial direction.

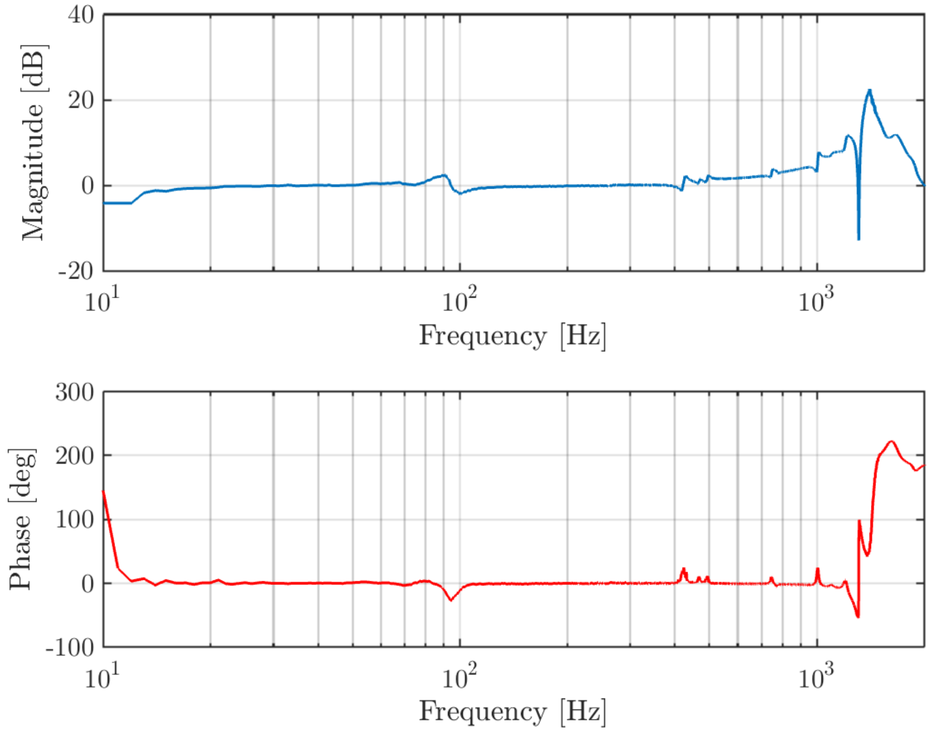

Figure 5.5: Transfer function for universal joint in torsional direction.

The phase shift around 100 Hz is due to the sleeve connected to the universal joint fishtailing. The sharp dip below the global max in magnitude has not been fully investigated but is believed to originate from the small clearance in the joint resonating.

5.1.2 Torsional Direction

The torsional excitation was created via an eccentric radial force close to the end of the cylinder as seen in Figure 4.4. The measured mobilities are found in Figure 5.6.

In the lower frequency region the mobility follows a typical mass dominated behavior with -6 dB/octave. The peak around 20 Hz is believed to origin from the rig suspension. The response between 400 Hz–500 Hz offers a bit of a challenge as there are two resonances close together and with slightly different behavior.

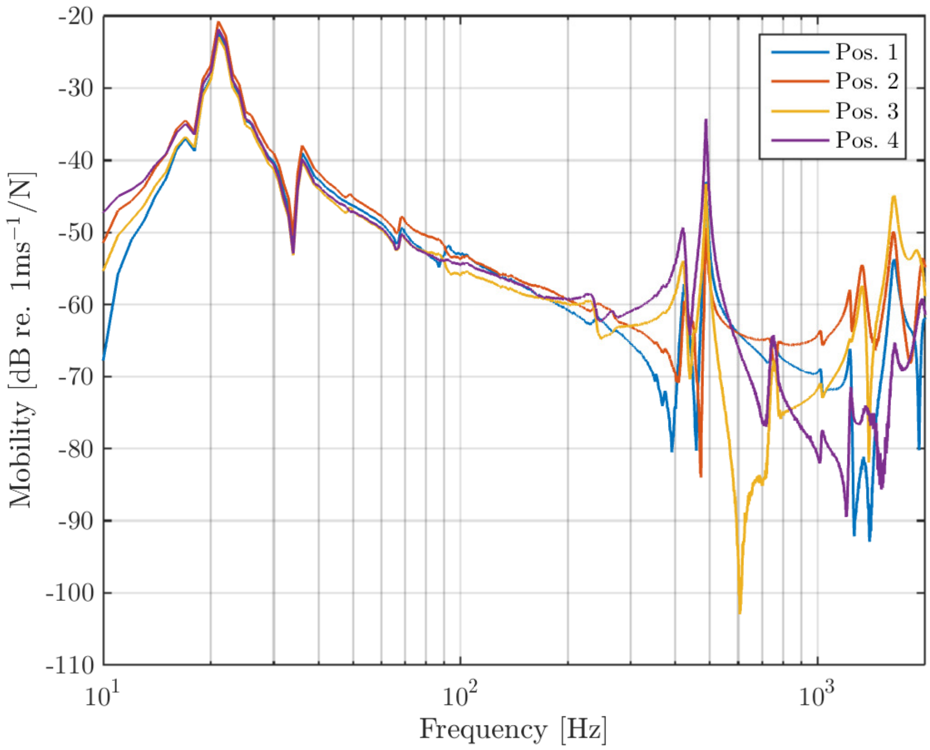

Figure 5.6: Measured input and transfer mobilities for fully extended standard shaft in tangential direction.

The resonance at 415 Hz is preceded by an anti-resonance in the input mobility while the transfer mobilities are not. This is expected and concludes that the behavior is spatially located between the point of excitation and the point where the response is measured, in contrast to any resonances originating from the universal joints. A very strong resonance is found at 490 Hz. The end to end motion is similar to the first mode of a freely suspended torsional mass spring system, masses being the universal joints with splined collets at each end. As observed in Figure 5.7 both piston and cylinder move in phase separately, but the end to end motion is out of phase by 180 deg due to the phase shift in the bearing. It seems likely that much of the end to end motion takes place across the bearing in this frequency region.

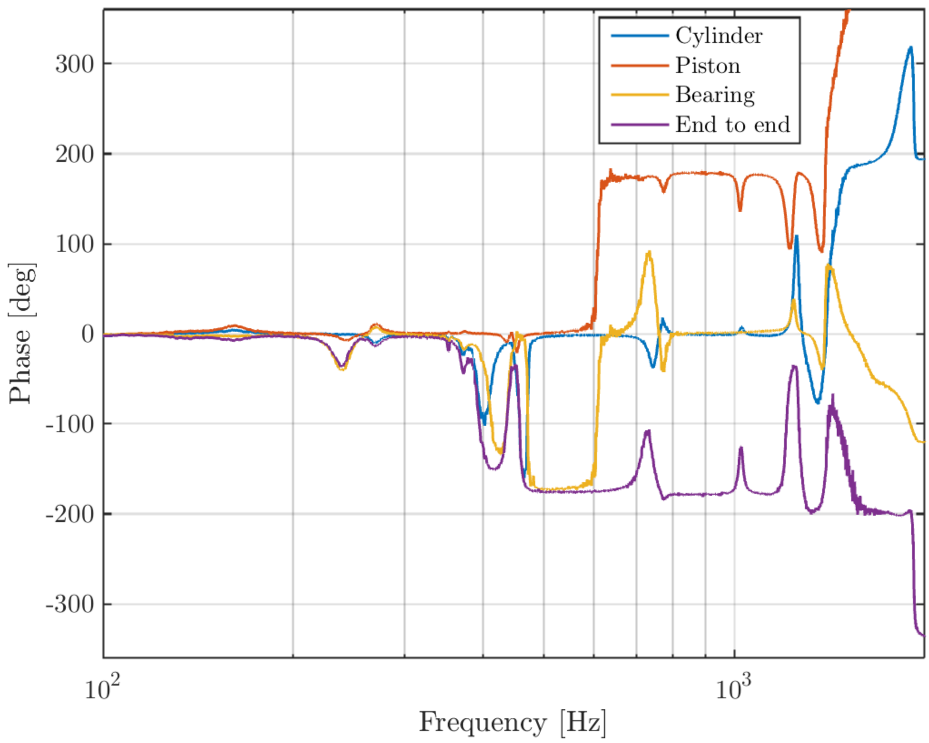

Figure 5.7: Transfer phases for the fully extended standard shaft in tangential direction.

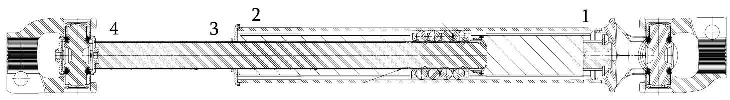

Figure 5.8: Measurement positions during torsional measurements.

The effect of increased effective length of the cylinder is noticeable around 500 Hz in Figure 5.9 as a consistent lowering of the resonance frequency to increase in telescope extension. Figure 5.9a show input mobility in Position 1. Figure 5.9b show transfer mobility to the far end, Position 4. The resonance around 400-450 Hz is even more sensitive to telescope position. For the 300 mm case this mode is not at all visible. As later shown in Figure 5.10 the mode shape looks like the first mode of a torsional mass spring system, clamped at the input end. This could explain why the resonance is very sensitive to telescope extension and sometimes does not show at all. This mode shape does theoretically have a node at the point of excitation. At 760 Hz a resonance independent of telescope extension is observed, this corresponds to the first mode of the piston.

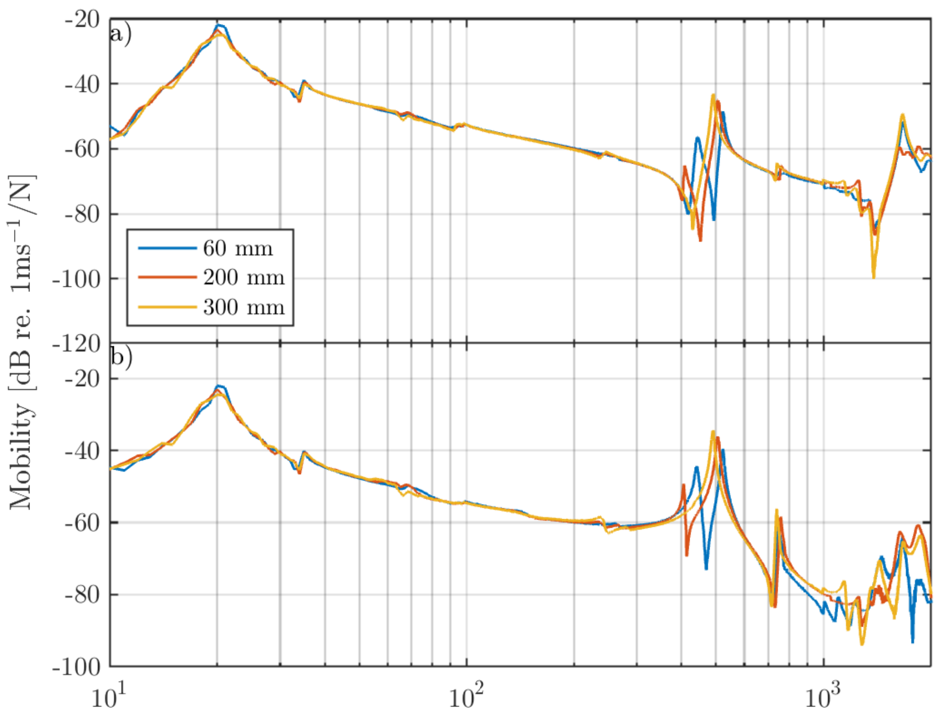

Figure 5.9: Measured a) - input and b) - transfer mobilities in torsional direction for three different telescope extensions.

In an additional measurement, ten points along the steering shaft were measured to capture the motion. This was done as a support in the analysis as higher spatial resolution was needed to fully understand the response. The data was imported to Matlab and visualised as a moving object sweeping angular displacement with respect to phase relation. In Figure 5.10 a single frame for each frequency can be observed. The frequencies were chosen from the behavior in Figure 5.6 and Figure 5.7. More elaborate plots containing ten timesteps for each frequency can be found in Appendix C.

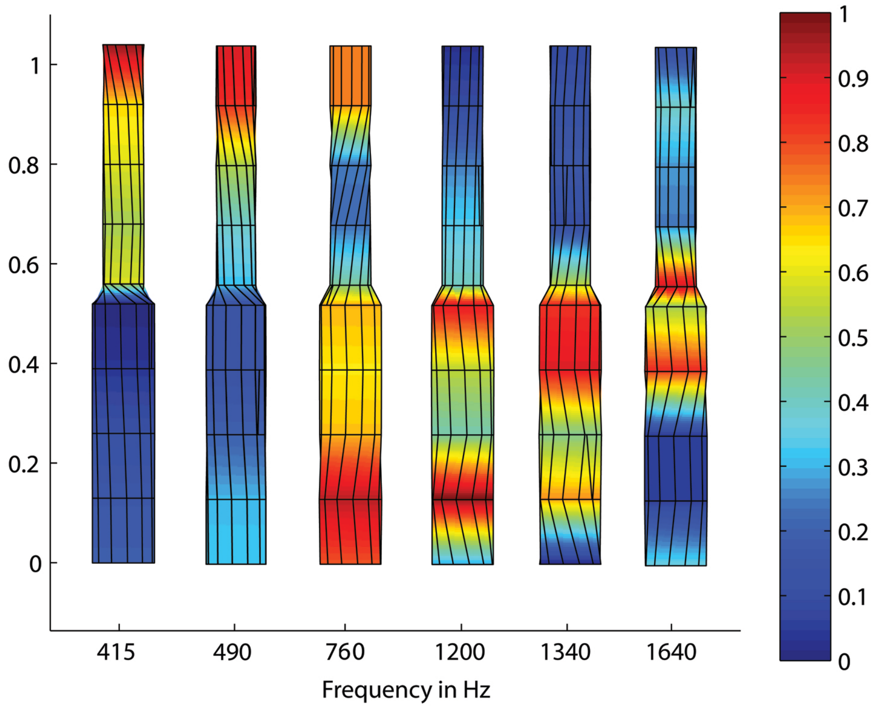

Figure 5.10: Visualisation of measured torsional motion for some frequencies. Excitation in y = 0, corresponding to Position 1. The colorbar scale indicates magnitude of the normalised angular displacement, the vertical contour lines are more clear in terms of angular gradient.

5.1.3 Radial Direction

The radial direction is the case most sensitive to the amount of piston extension. This is expected since moving the piston also means altering the position of contact between piston and cylinder. Geometry is also of great importance when it comes to torsional waves, but as bending wave modes appear much lower in frequency, the effect is clearer in the region of interest.

The case with 60 mm extension was found to produce the most resonant response and is shown in Figure 5.11 where Pos. 1 corresponds to input mobility.

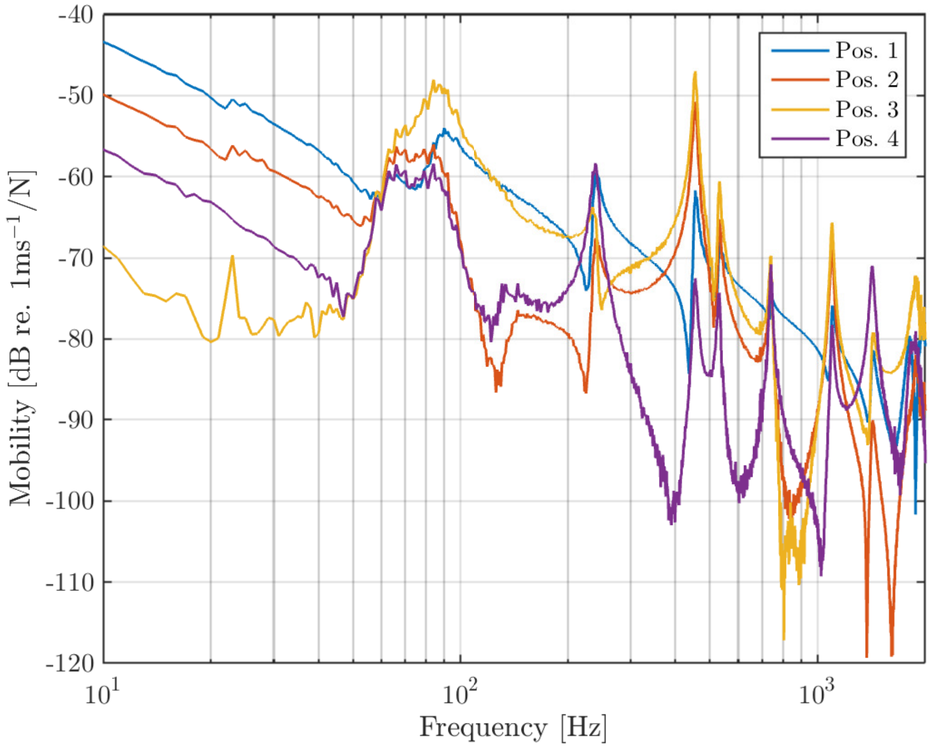

Figure 5.11: Measured Input and Transfer Mobilities for 60 mm extended standard shaft in radial direction.

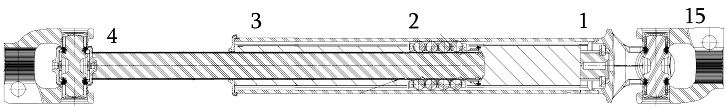

Figure 5.12: Measurement positions during radial measurements.

In Figure 5.13 the change in response when moving the point of connection between cylinder and piston is obvious. The 60 mm option is most likely to capture all individual modes as the subsystems are coupled in parallel rather than in series. The 240Hz and 740Hz resonance varies only in amplitude, not frequency. This is explained by the fact that these are the first and second mode of the piston. The change in amplitude is simply explained by the amount of energy transferred to the piston. The 420 Hz and 1100 Hz response on the other hand, belongs to the cylinder and therefore moves in frequency. This is because the cylinder is disturbed by the piston at different positions depending on the amount of extension, thus altering the mode shapes. The decrease in measurement quality around 80 Hz is believed to be due to the cylinder pivoting around the bearing. The scraper seal mounted to the outer end of the cylinder then clash with the piston causing distortion. This motion is later observed in Figure 5.14, but for a fully extended shaft.

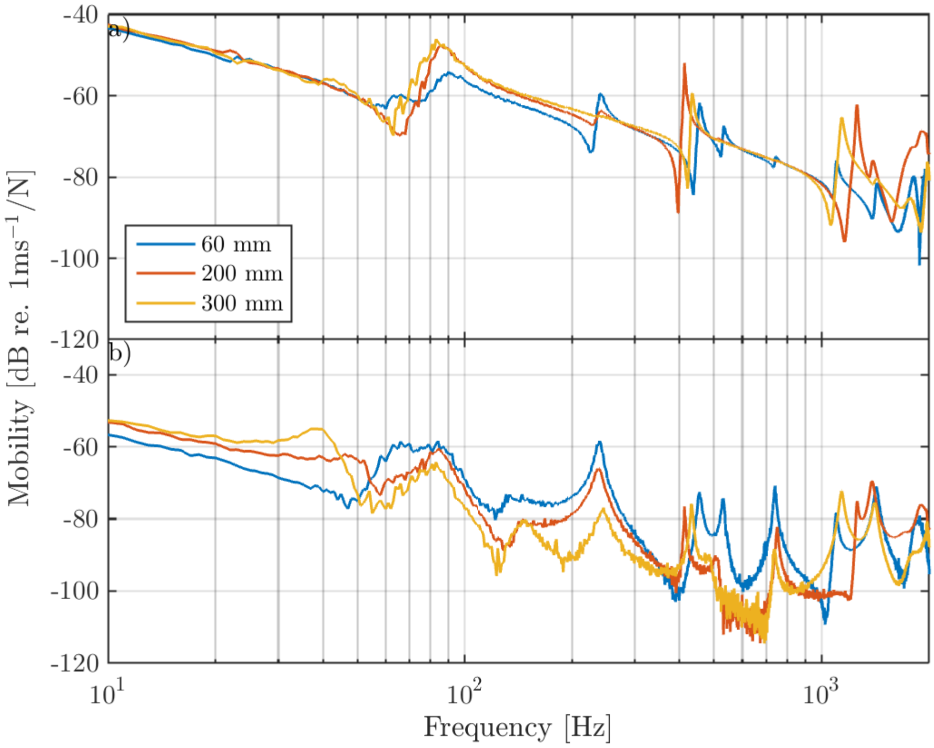

Figure 5.13: Measured a) - input and b) - transfer mobility in radial direction for three different telescope extensions.

The input mobility in Figure 5.11 is similar to that of bending waves on a beam. A closer observation reveals that there are modes present at both piston and cylinder even at lower frequencies as the modal pattern of a single beam does not fit. When looking at the 10 point visualisation in Figure 5.14 it is clear that the resonance at 240 Hz belongs to the first mode of the piston while the 420 Hz resonance couples to the first mode of the cylinder.

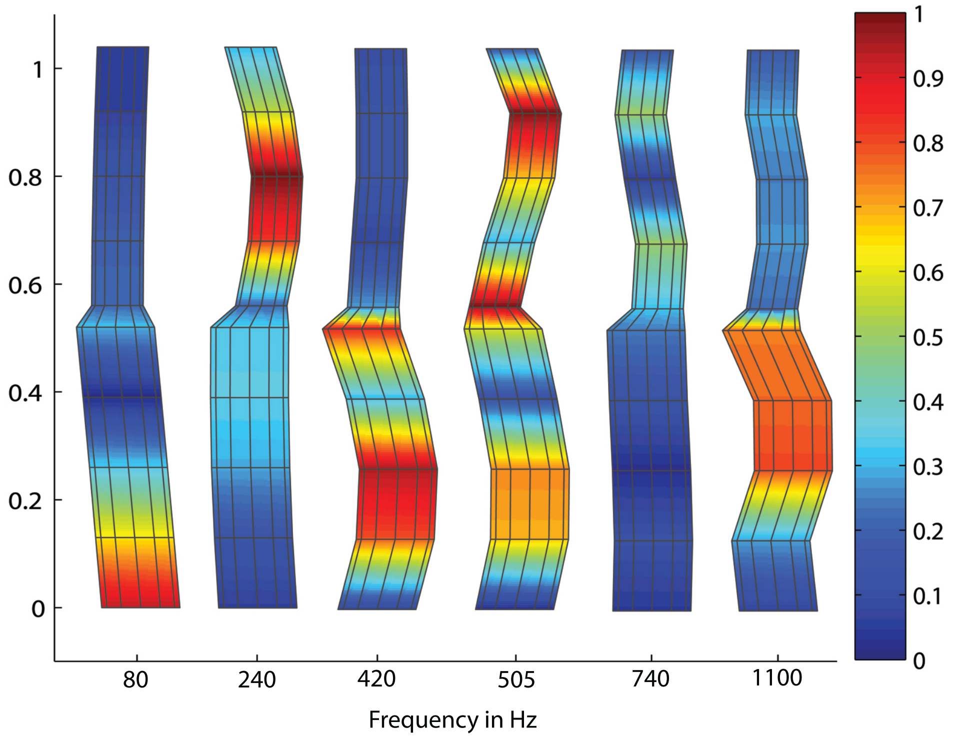

Figure 5.14: Visualisation of measured radial motion for some frequencies. Excitation in y = 0, corresponding to Position 1. The colorbar scale indicates magnitude of the normalised displacement.

5.1.4 Quality of Measurements

In general the shaker method is often a good way of achieving high quality measurements as the object under study is in steady state condition and data can be acquired with no respect to time restrictions or transient excitation.

Coherence

The coherence was monitored during the entire measurement process and the setup was occasionally geometrically tuned to achieve as high quality as possible. Coherence for data displayed Figure 5.2, Figure 5.6 and Figure 5.11 are found in Figure 5.15.

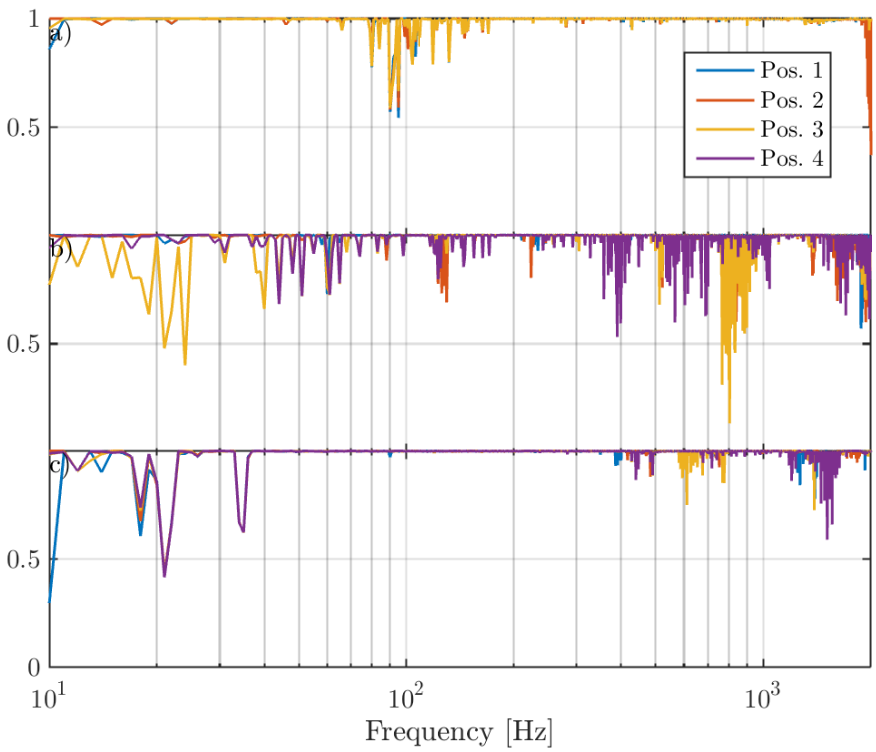

Figure 5.15: Typical coherence for data in the three axes.

Coupling of Wavetypes

The steering shaft does under many circumstances and in many frequency regions show great similarities to simple structures and models, such as mass spring systems and beams. However, there are also frequency regions where the behaviour is more complex and strong coupling between wave types is inevitable. Figure 5.16 show mobility in all three axes but with force reference i.e excitation in a) - axial, b) - torsional and c) - radial direction respectively. All data concerns Position 1 with a telescope extension of 60 mm.

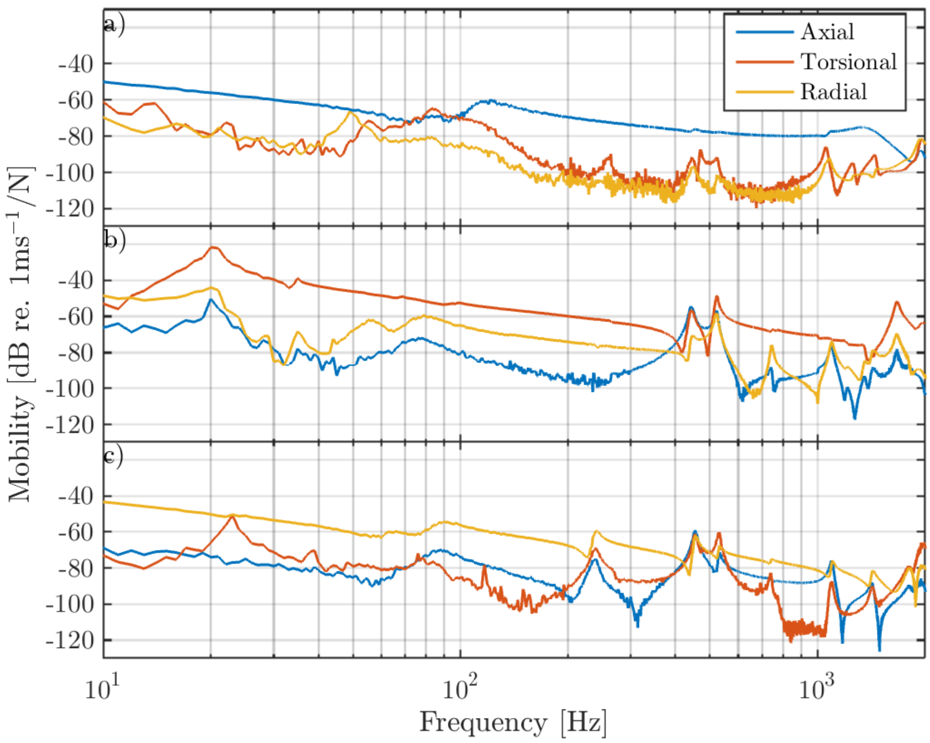

Figure 5.16: Coupling to other directions in Position 1 when exciting: a) - axial, b) - torsional and c) - radial

Figure 5.16a), shows that axial excitation and longitudinal waves is the type least prone to couple to the other wave types. Good separation is obtained through out the spectra besides around 100 Hz, coupled to the bearing resonance in axial direction. This is to some extent expected as this case is also the easiest when it comes to achieving proper alignment of the system. Misalignment between either the stinger and steering shaft or universal joint to main body will result in eccentric forces or masses, thus creating cross coupling. In the case of torsional waves the eccentric stinger attachment, such misalignment is foreseen. As this was the only solution applicable, it will have to be accepted.

Regarding Figure 5.16b) and c), there is an interesting region around 450Hz–550 Hz. Both torsional and radial excitation also excite both other axes to similar velocity levels as the main axis, sometimes even higher. Such strong coupling, especially to axial motion, was not expected. This behaviour is believed to be caused by the lower universal joint even though the exact mechanism and motion of the joint is yet to be explained. The response of the joint can be further studied as mobility in Figure 5.20 and as transfer function and phase in Figure 5.21. During these measurements it was also proven that the strong coupling remains even with the steering gear attached. The response is consequently not something caused by the joint being freely suspended.

How excitation in one axis result in different vibration levels is not the only parameter to investigate regarding coupling of wave types. Also how the vibrations in a certain point and axis depends on the direction of excitation should be examined. Some very interesting results should be highlighted from this analysis. From Figure 5.17a) the conclusion is drawn that axial excitation does not in fact produce the strongest axial response in Position 4. Instead torsional excitation seem to create levels up to 40 dB higher. In Figure 5.17c) the same phenomena is visible at 240 Hz as radial excitation produces the highest torsional vibration level. The levels are presented as mobility and the input force will differ depending on the direction of excitation. The APS does however show similar relative levels and can be found in Appendix C.

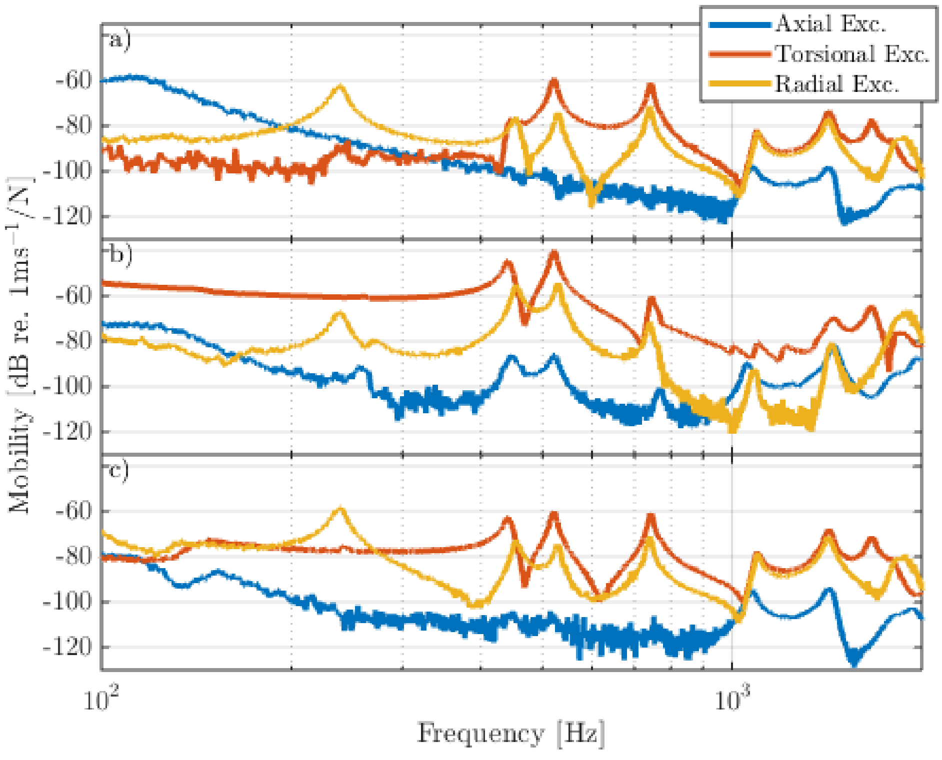

Figure 5.17: Comparison of mobilities in Position 4 when exciting in different directions. a) - axial velocity, b) - torsional velocity and c) - radial velocity.

5.1.5 Mobility Measurement With Steering Gear Attached

As a preparatory measurement it was decided to carry out measurements with the standard shaft hanging in the same rig as during previous measurements, but this time with a steering gear attached. This experiment was conducted mainly to see whether the shaker was powerful enough to be used in the vehicle measurements and also to understand the influence of the steering gear. The steering gear was filled with oil and attached rigidly to the steering shaft as seen in Figure 5.18.

Figure 5.18: Measurement setup with steering gear attached, here in torsional configuration.

Although the steering gear is very heavy compared to the steering shaft, the influence is not as great as expected. The spring like characteristics of the valve control torsion rod is observed clearly in Figure 5.19, from 10 Hz up to a highly damped resonance at roughly 100 Hz. From 200 Hz the steering gear influence is mostly by added damping. This means that the mass on the shaft side of the torsion rod is relatively small.

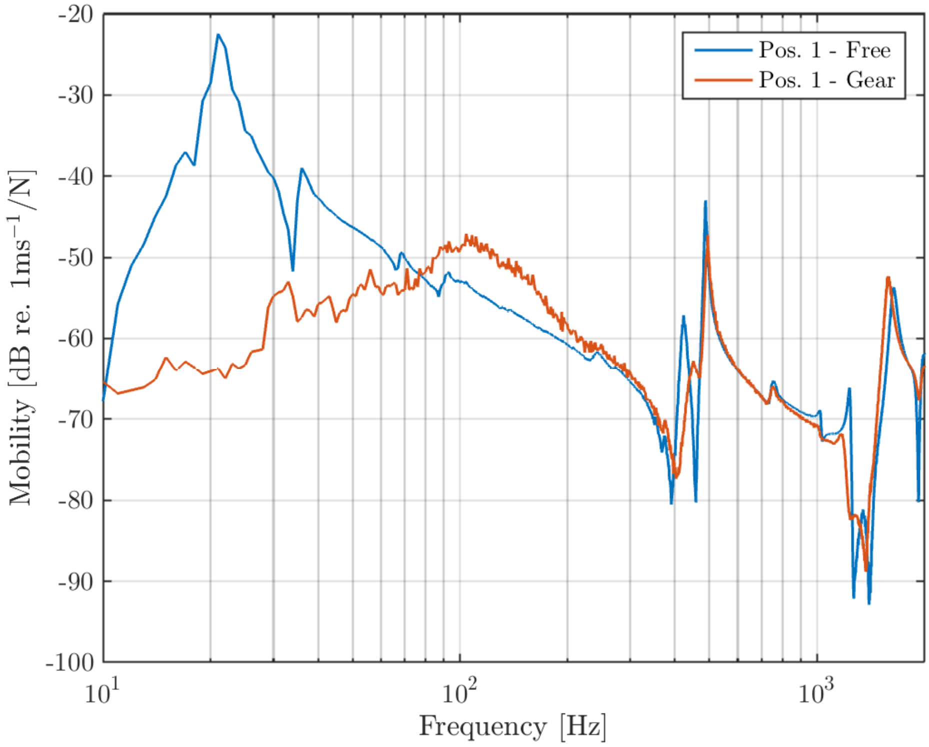

Figure 5.19: Comparing torsional input mobility with steering gear attached to free condition, shaft fully extended.

It should be stated that the steering gear was not attached to the floor in any way in the radial measurements but simply held in place by its own weight. However, two measurement points on the steering gear used as reference show that velocity on the gear housing is roughly 20 dB lower than on shaft itself. The influence from the steering gear is clearly observed in Figure 5.20. The mass of the steering gear is substantial compared to the steering shaft, the asymptotic slope from 10 - 200 Hz does however again indicate an increase in stiffness rather than mass compared to the freely suspended case. The cause of the resonances in the low frequency region are difficult to derive as they could be caused by a number of mechanisms. Observing Figure 5.18, it is plausible that the shaft on one side and the steering gear on the other would bend around the universal joint resulting in a resonant response similar to the fishtailing previously observed from the lower universal joint. Adding mass to the end of the shaft should also substantially lower the bending wave resonances on the shaft itself. The influence of the steering gear torsion rod could also influence the response, the mechanic properties of the gear is however unknown at this point. The validity of the low frequency influence will be deduced during the in-vehicle measurements.

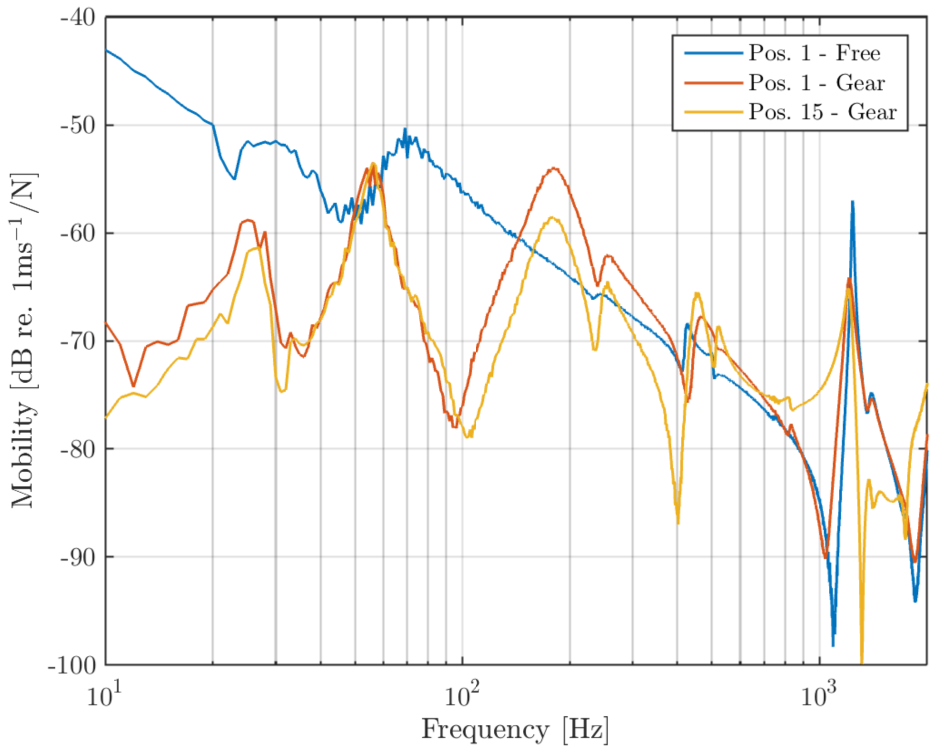

Figure 5.20: Comparing radial input mobility with steering gear attached to free condition, shaft fully extended.

The measurement produced the opportunity of studying the response of the lower universal joint also in radial direction, as Position 15 in Figure 5.20 and as transfer function with magnitude and phase in Figure 5.21. A strong resonance in the joint is found in both figures around 1100 Hz.

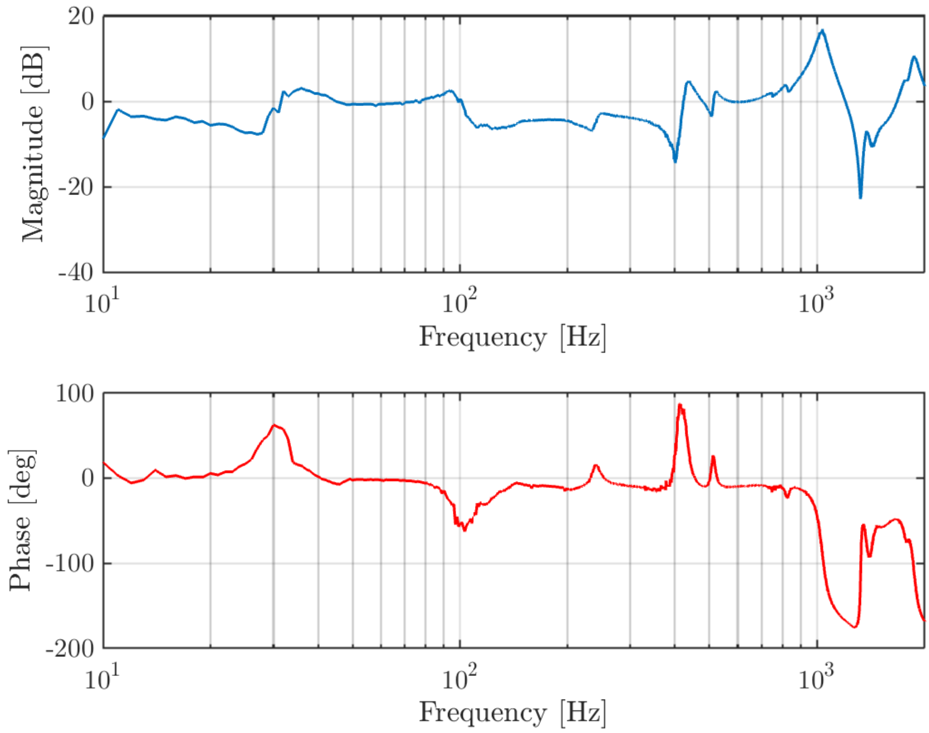

Figure 5.21: Transfer function for universal joint in radial direction, steering gear attached.

5.2 Prototype Shafts

Both prototypes investigated has undergone the same basic measurements as the standard shaft. All three axes were excited in consecutive measurements and with the same extensions as previously stated. The measurement points hold the same geometry as for the standard shaft. This chapter will present some of the measurements where the behavioural trends and response is most deviant from the standard shaft.

During measurements with 300 mm extension the NVH shaft had to be locked as it is designed to contract when released, though with low force. This was achieved by a few turns of masking tape around the piston. Making contact with the polyurethane dust seal the tape acts as a stop while keeping the mechanical coupling between piston and cylinder to a minimum.

5.2.1 Axial Direction

Looking at Figure 5.22 it is obvious that both prototypes are more resonant than the standard shaft in the higher frequency region. The added mass lowers the transfer mobility slightly up to around 200Hz, while the NVH prototype lies higher through out the spectra. No tape was used on the NVH shaft in this measurement.

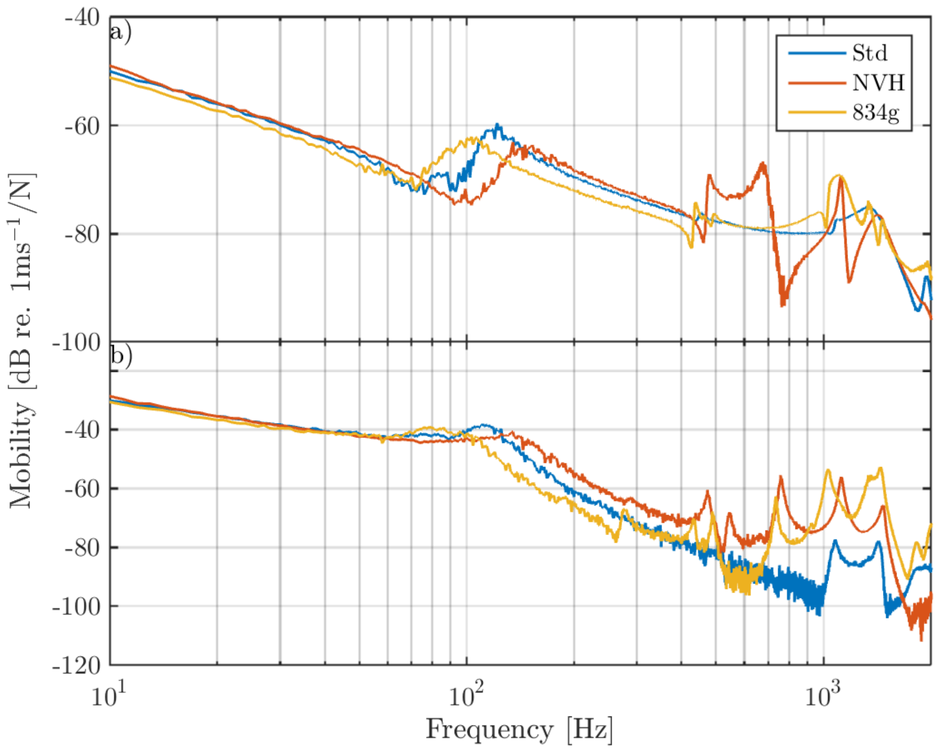

Figure 5.22: Standard shaft compared to the two prototypes in axial direction, extension 60 mm. a, Position 1 and b, Position 4.

5.2.2 Tangential Direction

Observing the torsional response in Figure 5.23, the shaft with added mass has a very protruding behavior from 450 Hz and above. The clear response is believed to origin from the first modes of the piston, as is it constant in frequency with different extensions. A rather big improvement is achieved by the anti resonance in the 500 Hz–800 Hz region, this is however likely to change when mounted as more mass is added to the piston side. The extra mass in the 834g prototype also shows as a rather constant -2.5 dB offset in the mass dominated region up to 300 Hz.

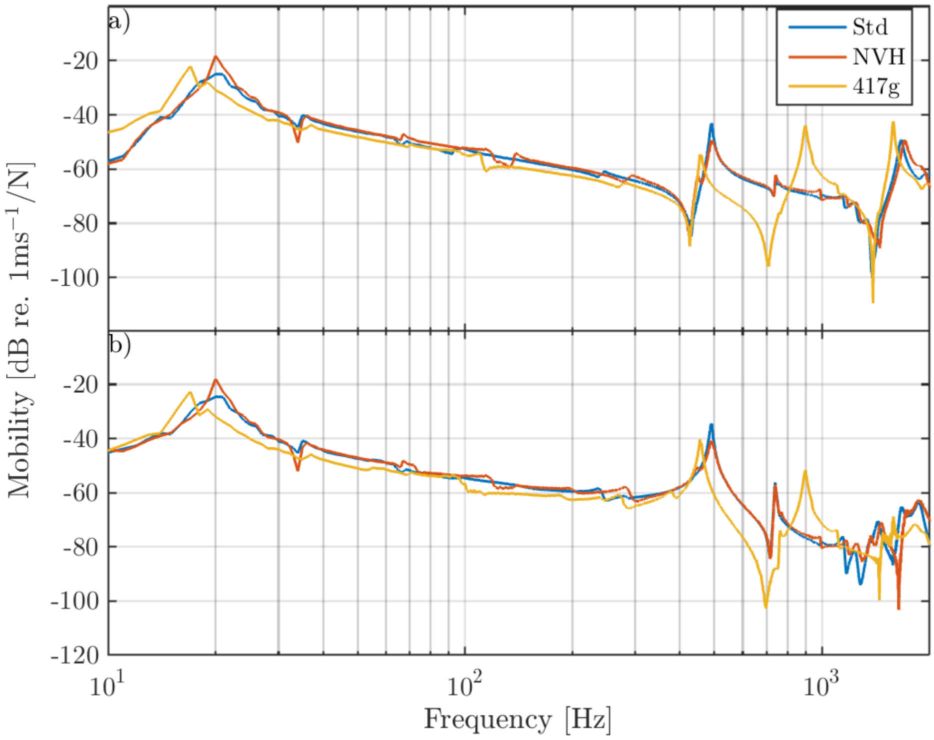

Figure 5.23: Standard shaft compared to the two prototypes in torsional direction, extension 300 mm. a, Position 1 and b, Position 4.

5.2.3 Radial Direction

Again the added mass on the 834g prototype is visible as a drop in mobility at lower frequencies in Figure 5.24. The small advantage however soon disappears and the effect is instead observed as a shift in resonance frequencies and slightly reduced damping compared to the standard shaft. The NVH shaft produces a response very similar to the standard shaft above 700 Hz. Below that the transfer mobility is generally higher as the first resonances lies higher in frequency.

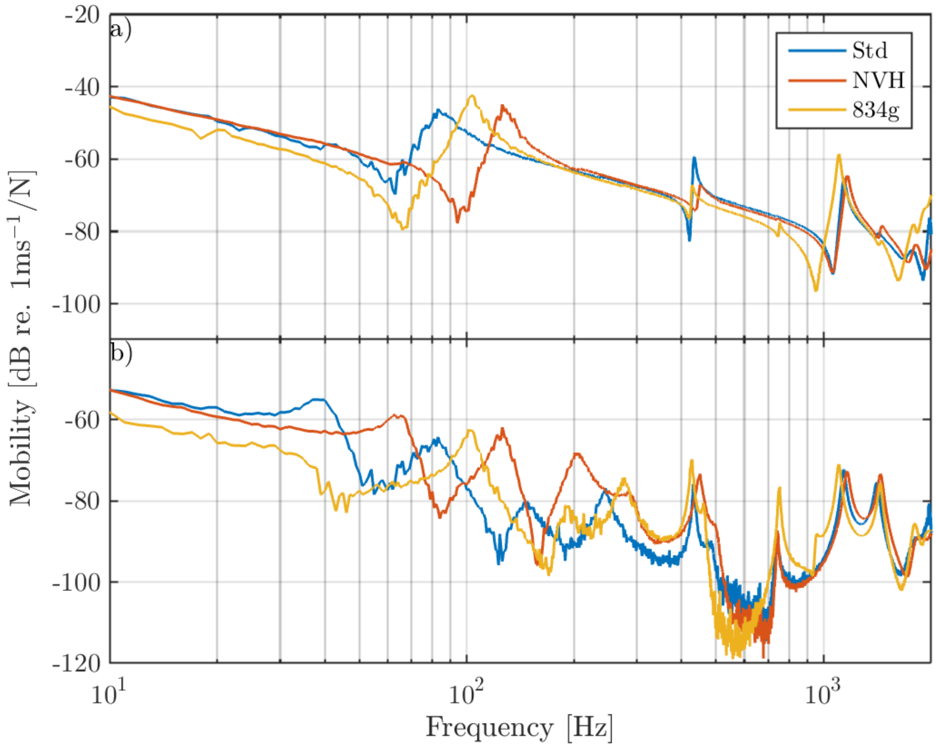

Figure 5.24: Standard shaft compared to the two prototypes in radial direction, extension 300 mm. a, Position 1 and b, Position 4.

5.2.4 Prototype Shafts Conclusions

After comparing the two prototypes to the standard shaft it is clear that there are no noticeable advantages drawn to any of them in an isolated condition.

834g Shaft

The 834g added to an otherwise unaltered standard shaft is far to little to improve the performance in terms of shear mass loading. It is possible that mass could be added lo lessen the impact of some specific resonance, if properly tuned in weight and placement. As of now the mass seem to somewhat improve the region 550 Hz–800 Hz in tangential direction. If this was indeed the intention, the design could be improved by increasing the radius of the mass, thus increasing the mass inertia of the shaft. When taking the other directions under consideration, no improvement could be validated.

NVH Shaft

The NVH prototype shows a response very similar to the standard shaft in tangential direction with no noticeable differences. In axial direction the performance is generally worse with a highly resonant behavior above 450 Hz. The bearing resonance in slightly more damped but instead pushed up in frequency. The same features hold also for radial direction and bending waves as the NVH shaft seems stiffer and less damped than the original. As of now there is no reason to believe that this prototype would perform better when mounted.

Chapter 6

In Vehicle

All in vehicle measurements take place in the semi anechoic chamber at Volvo GTT Noise & Vibration Laboratory.

6.1 The Vehicle

The vehicle under study is a previous field test Volvo 2012 6x4 FH13 timber truck. Since previous tests involved driveline durability, engine and transmission were removed. This means that some changes to the stiffness of the frame and also in the total damping of the chassis has been done. These changes are however estimated to have negligible impact on the transfer path of interest in this study. The full configuration of the vehicle can be seen in Table B.1

6.2 Measurement Setup

The different steering shafts are subjected to the same tests as in the previous measurements where the shafts were excited in torsional and radial direction. The shaker was both rigidly attached to the steering gear mount as seen in Figure 6.1, and hung up in strings and a rubber strap Figure 6.2.

Figure 6.1: Shaker mounted to the truck.

During these measurements both vibration velocity and radiated sound were measured. The shaker itself was wrapped in bitumen foiled damping mats to avoid high levels of direct noise source radiation. Early testing showed that the energy input was high enough to create audible sound inside the cab when applying a sine frequency sweep.

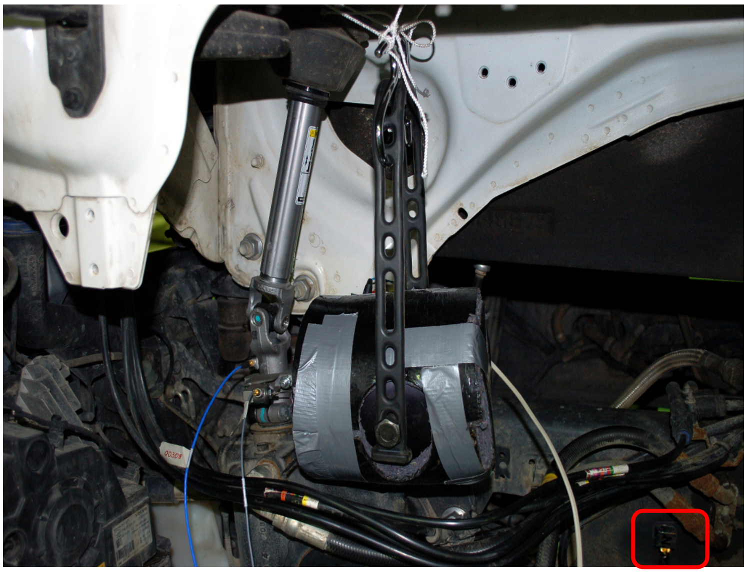

Figure 6.2: Shaker in hanging setup. The frame mounted accelerometer can be seen inside the red rectangle.

Three microphones inside the cab were used to record radiated sound and to monitor the spatial spread in noise level. One above the steering wheel as in previous tests, this position is close to the position of the drivers head. One at the approximate location of the passengers head and one 0,5m below the sun roof. A reference microphone outside the cab were used in all measurements.

The accelerometers were mounted on the steering shaft, dashboard, frame, steering column and just below the steering wheel. The setup can be seen in Figure 6.3. The dashboard mounted accelerometer was set 2/5th in on the panel and centered to the radius of the steering wheel. The accelerometer on the steering column is mounted on the main body of the mechanism and is marked with a red dot in Figure 2.4.

Figure 6.3: The basic setup for in-vehicle measurements.

Chapter 7

Analysis – In Vehicle

All total levels presented in this chapter are based on the frequency range 100 Hz - 1 kHz. All sound pressure levels presented are A-weighted other than when in direct comparison to velocity. Two steering wheel positions are evaluated. The upright position refers to column and neck tilt adjusted in an as close to straight line continuation of the steering shaft as possible, typical for entering and exiting the cab. The telescope extension is in this case around 250 mm.

In the driving position the steering wheel is set to a comfortable setup for driving. Both upper universal joints is at a slight angle and the telescope extension is approximately 150 mm. The 834g shaft was not excited in radial direction as there was not enough room to fit the mount.

7.1 Prototype shafts

This section will be dedicated to a comparison between the shaft under study. With the complete system in place not only vibrational properties but also sound radiation is taken under consideration.

7.1.1 Mobility

Transfer mobilities presented in this section refer to position 4 as this is the furthest position where acceptable isolation between wave types is still maintained. Transfer mobilities to a point just below the steering wheel show similar levels in all three directions, meaning that the level of cross coupling is very strong and therefore only total velocity level can be considered. Such transfer mobility can be found in Appendix C. Two positions on the steering shaft were used, corresponding to input and transfer mobility.

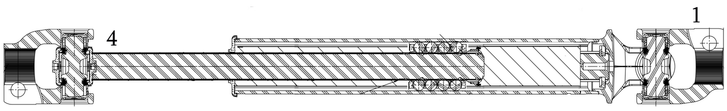

Figure 7.1: Measurement positions during in vehicle measurements.

The basic vibrational properties of the vehicle mounted shaft prototypes can be observed in Figure 7.2 with torsional excitation and Figure 7.3 with radial excitation.

Subplot a) show the input mobility and b) the end-to-end transfer mobility for each shaft. The curve 'Std*' refers to the measurement with standard shaft disconnected from the steering column.

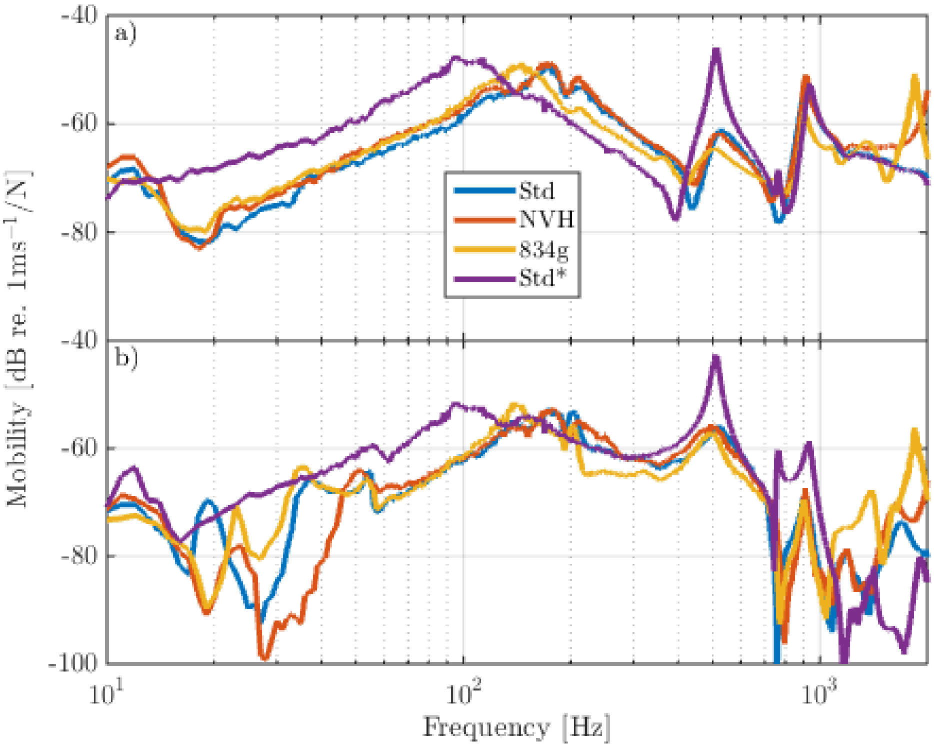

Figure 7.2: a) - input mobility and b) - transfer mobility of the three shafts in torsional direction with upright steering wheel position.

The inertia of the steering wheel shows in the lower frequency range a constant lowering of the input mobility compared to the 'Std*' case. The steering wheel also introduce damping to the otherwise sharp resonance around 500 Hz.

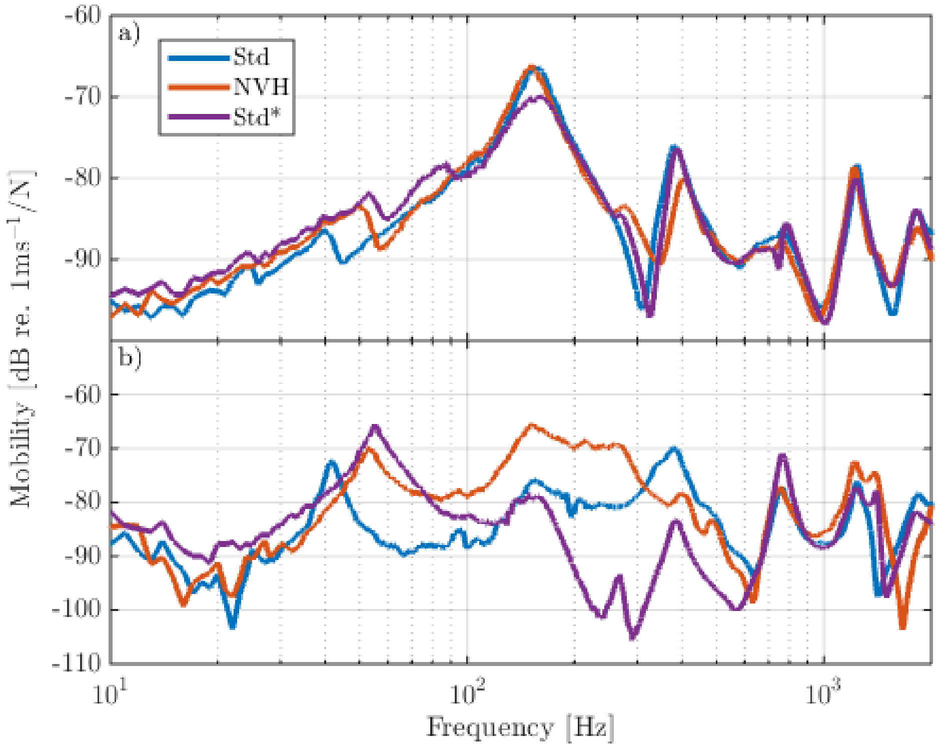

Figure 7.3: a) - input mobility and b) - transfer mobility of the standard and NVH shafts in radial direction with upright steering wheel position.

The transfer mobility in Figure 7.3b) show a constant 10 dB offset between the two shafts in the 50 - 300 Hz region, a trend also recognised from the freely suspended measurements. Regarding the standard shaft the more pronounced resonance at 400 Hz is also visible in the transfer mobility and was previously concluded to belong to the first mode of the shaft cylinder. The 834g shaft does lower the mobility slightly in the 150 - 300 Hz region, higher levels are however found above 1 kHz compared to the other shaft. These differences in transfer mobility can to a certain extent also be identified in the radiated noise.

7.1.2 Radiated Noise

Throughout all measurements the radiated noise inside the cab were recorded. These can be observed in Figure 7.4 and Figure 7.5, where a) is the upright position and b) the driving position.

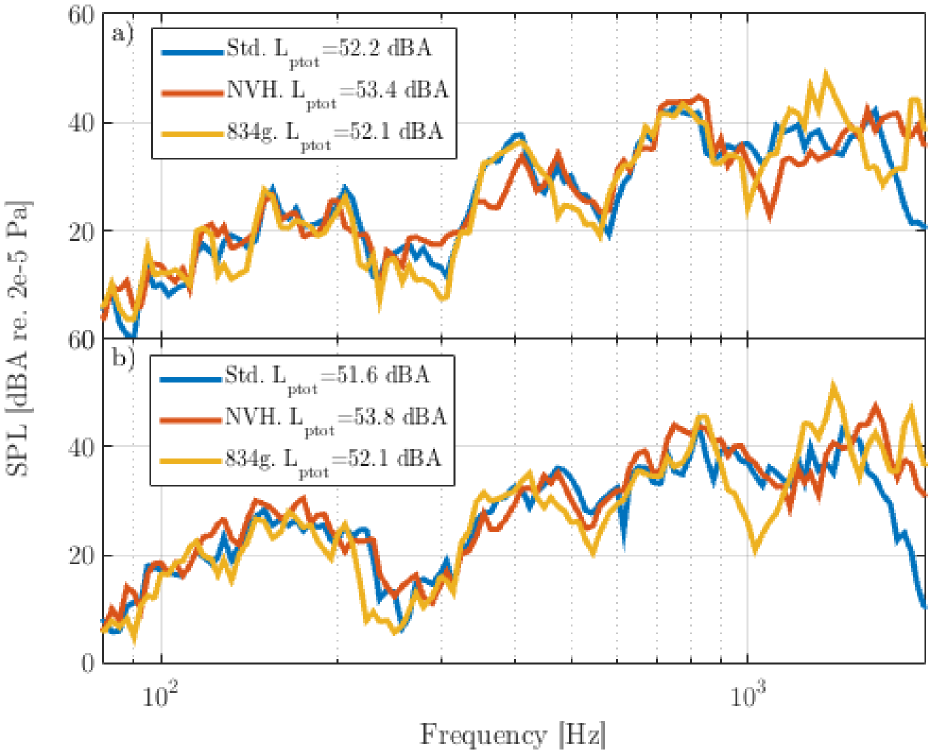

Figure 7.4: Averaged sound pressure level inside the cab for torsional excitation of different shaft prototypes. Comparison between a) - upright position and b) - driving position.

The NVH Shaft produce slightly higher noise level below 300 Hz but performs better than the other shafts in 300-400 Hz region. This behaviour is more clear in the upright steering wheel position and holds for both torsional and radial excitation. The correlation to radial transfer mobility is rather good concerning relative levels. The torsional transfer mobility however does not show the same correlation. This might provide some information on which wave types are relevant in the sense of sound radiation and will be investigated further in this report.

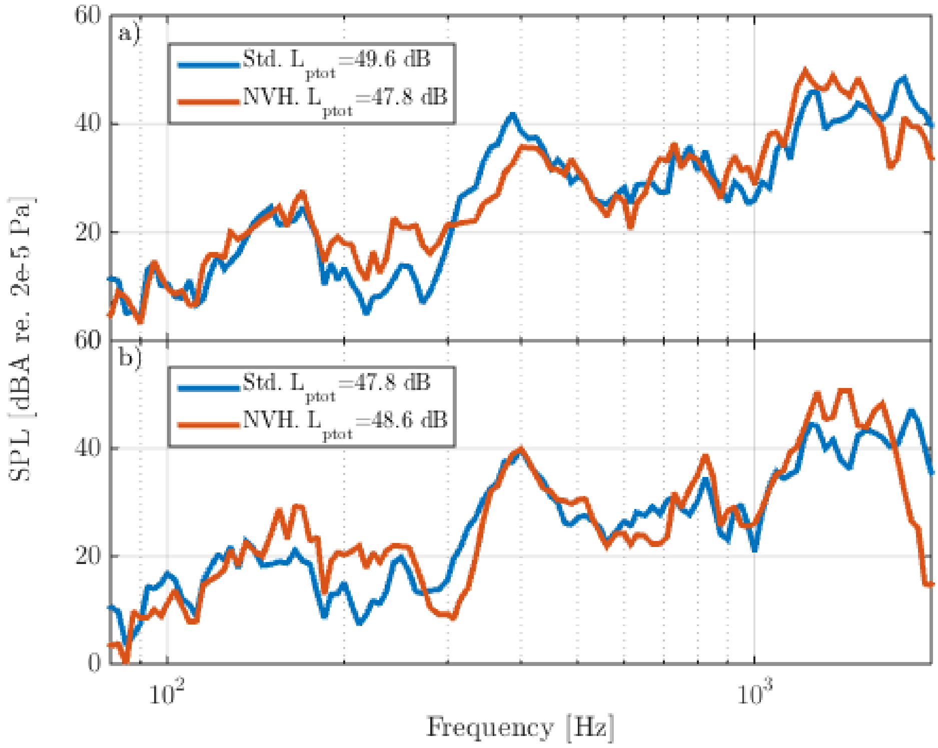

Figure 7.5: Averaged sound pressure levels inside the cab for radial excitation of different shaft prototypes. Comparison between a) - upright position and b) - driving position.

In general it can be said that the difference in the resulting sound pressure levels between the shafts are within 2 dB in range. None of the shaft are consequently performing better or worse, this depends on the positioning of the steering wheel as well as type of excitation. It should also be noted that the difference between the shafts are in the same order as the difference generated by changing the steering wheel position from upright to driving position. An estimated Test-Retest variability of 0.5 dB should also be accounted for.

7.2 Transfer paths and individual contributors to the total noise level

When comparing the radiated sound from different setups, it is possible to obtain some information on individual contributions from radiators as well as how the transfer paths contribute to the total level. Figure 7.6 shows the averaged sound pressure levels in four different configurations. ‘Frame Exc’ refers to the shaker rigidly attached to the steering gear, working under no load with the steering shaft completely removed and the resulting opening covered as seen in Figure 6.1.

‘Shaft Disconnected’ means that the steering shaft is disconnected from the steering column and the shaker is freely suspended. ‘STD Shaft Upright’ refers to the measurement with the standard steering shaft and the column in an upright position.

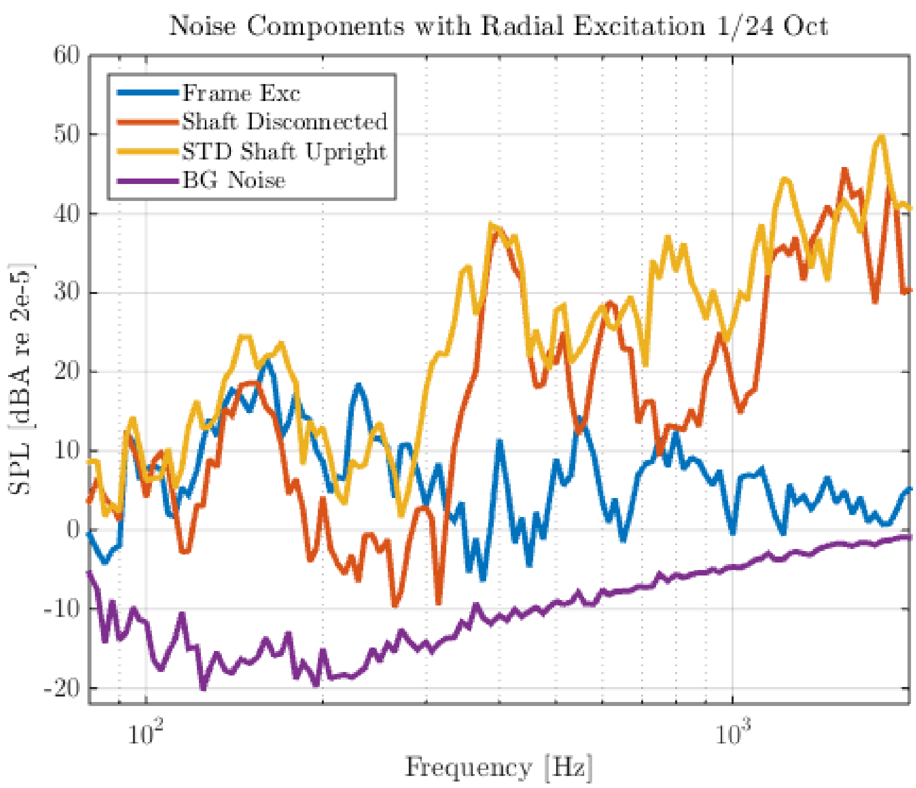

Figure 7.6: Averaged sound pressure levels inside the cab in four different configurations.

The shaft itself appears to be one of the main radiators from around 360 Hz up to around 500 Hz. Higher in frequency the shaft contribution alone is piecewise very close to the total level. This level of radiation is believed to originate from the resonance in the shaft bearing found during previous analyzes. Comparing the decoupled shaft to the standard case points towards that the main energy transfer path below 110Hz is via the cab suspension rather than the steering shaft.

A comparison how the velocity level change in different locations between the configurations, displayed in Figure 7.6, is of interest to further examine the transfer paths in the lower frequency region. Four such points are presented in Figure 7.7 and Figure 7.8. The point on the dashboard only covers vertical or bending wave velocity while the other three are three axis vector summations.

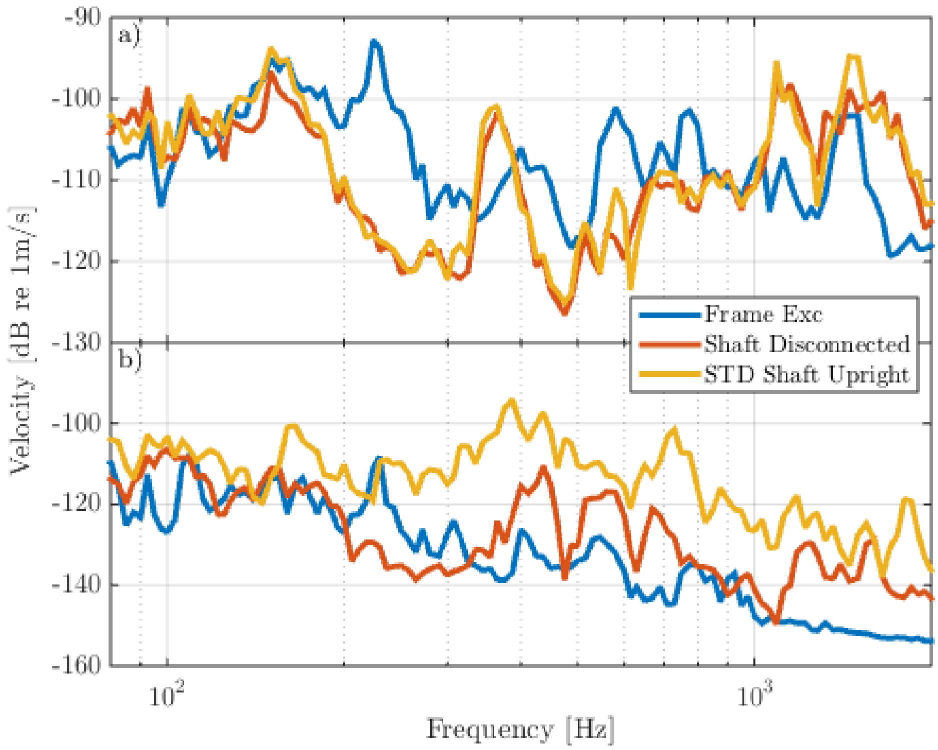

Figure 7.7: Total velocity levels in a) - frame and b) - dashboard

From Figure 7.7 relevant information is obtained when comparing the increase in velocity level on the frame at 230 Hz to the corresponding increase in noise level in Figure 7.6. It is clear that the cab suspension still transfers vibrational energy to some extent but can no longer be considered a contributing transfer path in terms of the whining noise. The cab suspension path and steering shaft path seem to be equally weighted around 150 Hz as the disconnected shaft case reduces the total level by approximately 3 dB and the levels on the frame are close to identical. This explains why differences in steering shaft mobility in the low frequency region does not show in the radiated noise.

When observing the dashboard the levels are higher than expected in the 'Shaft

Disconnected' case. There is no structure borne transmission from steering shaft to dashboard other than via the frame in this case. A higher velocity on the frame should result in a corresponding increase on the dashboard as there is no direct change in transfer paths when comparing the cases 'Frame' and 'Shaft Disconnected'. Further analysis point towards that the relative increase in levels of vibration on the dashboard is in fact generated by the airborne noise radiated from the steering shaft in this setup. This is supported by the weak coupling regarding velocity level from frame to dashboard in this frequency region, as noticed when comparing Figure 7.7 a) to b).

Figure 7.7 confirms that the frame is the dominating transfer path in the lower frequency region. Very large deviation is obtained on both column and steering wheel but the radiated noise show similar levels. The fact that the case 'Shaft Disconnected' produce similar levels as the case 'STD Shaft' at 100 Hz is believed to be due to the string between shaft and column used to keep the telescope from retracting.

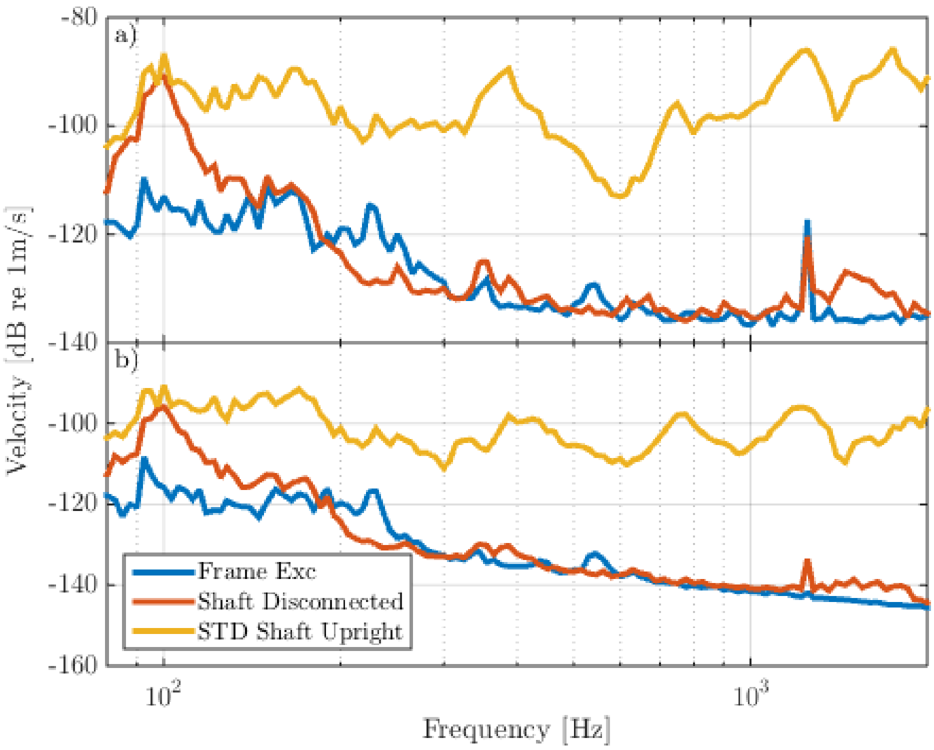

Figure 7.8: Total velocity level in a) - steering column and b) - steering wheel

When studying Figure 7.9 it becomes obvious that the shaft itself is radiating noise. The shaft is shielded with dense glass wool pipe insulation and there is little difference in structural load or damping between the two cases. The shielding is far from perfect and does not eliminate the shaft as a contributor completely, the effect is however clearly visible.

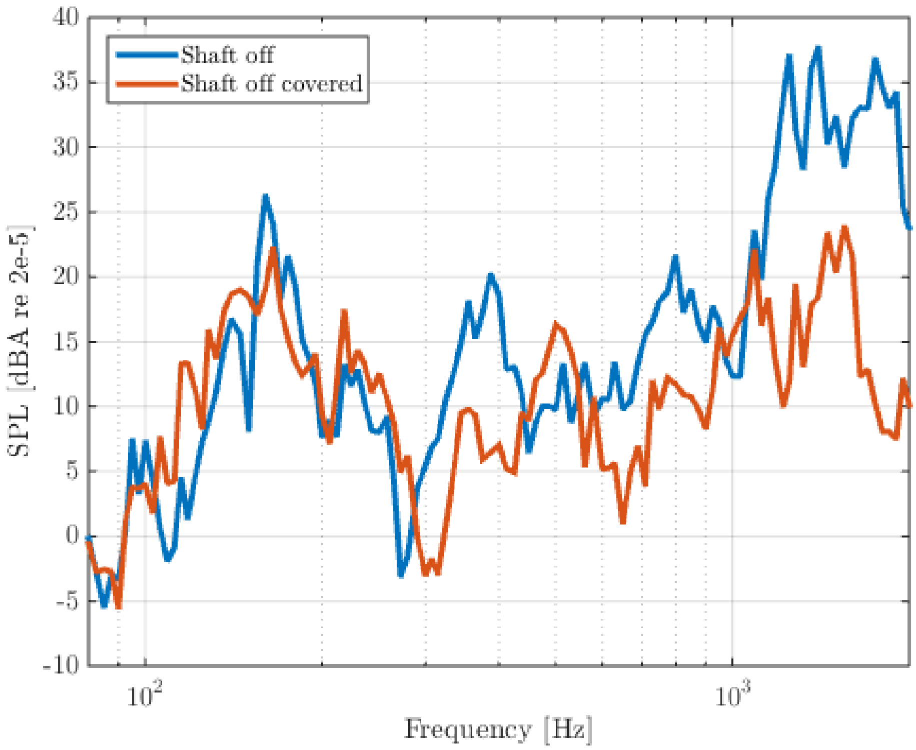

Figure 7.9: Averaged sound pressure levels inside the cab with the decoupled steering shaft covered.

7.3 Velocity level to noise level

It is an accepted fact that bending waves is the wave type to focus on considering direct noise radiation. When working with a transfer path in a complex geometry such as a cab interior there is no easy way of knowing how the wave types may couple later on. This section is therefore dedicated to finding how velocities in different directions correlate to the radiated noise. This type of information is important in order to successfully carry out modifications to the shaft or any other component close to the source.

Figure 7.10 show axial, torsional and radial velocity in pos 4 compared to radiated noise with both radial and torsional excitation. Steering wheel is here in upright position. Position 4 is out of all the positions measured upon the one with best correlation to radiated noise.

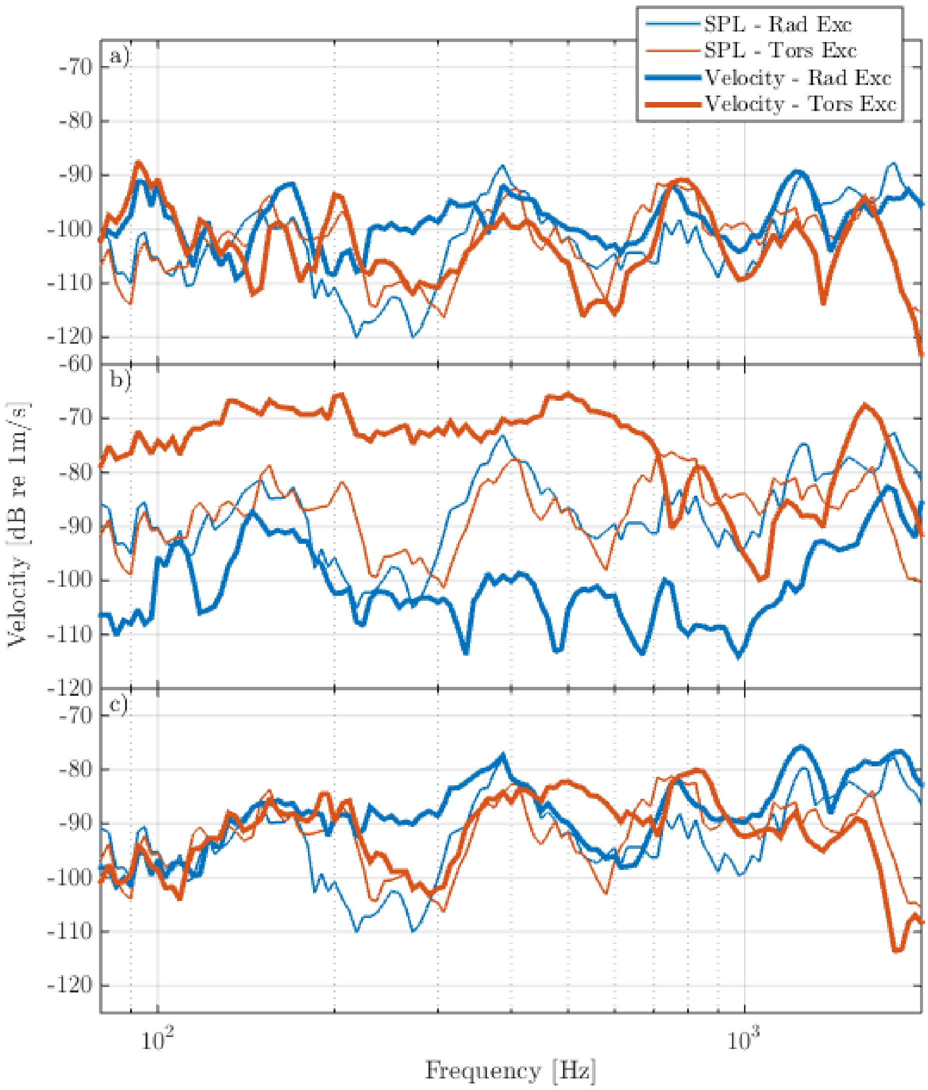

Figure 7.10: Velocity levels below the upper joint of the steering shaft in a) - axial, b) - torsional and c) - radial direction. Noise levels shifted down for reference.

Both axial and radial direction seem to correlate rather well with the sound radiation. Torsional direction on the other hand differ by 20 - 30 dB with similar noise level output. This means that torsional waves are not contributing to the noise radiation nor couple to other wave types within the system as the torsional velocity level is typically 20-30 dB higher than radial and axial in the case with torsional excitation. This also means that total velocity level on the steering shaft is a poor quantity to measure in terms of noise radiation. Bending wave velocity is around 10 dB higher than longitudinal wave velocity throughout the spectra.

7.4 System Non-linearity

To resemble the ideal case of the hydraulic excitation at 550 rpm, a pure sine wave at 177 Hz was used as input signal to the shaker. Figure 7.11 show very little distortion at this particular frequency.

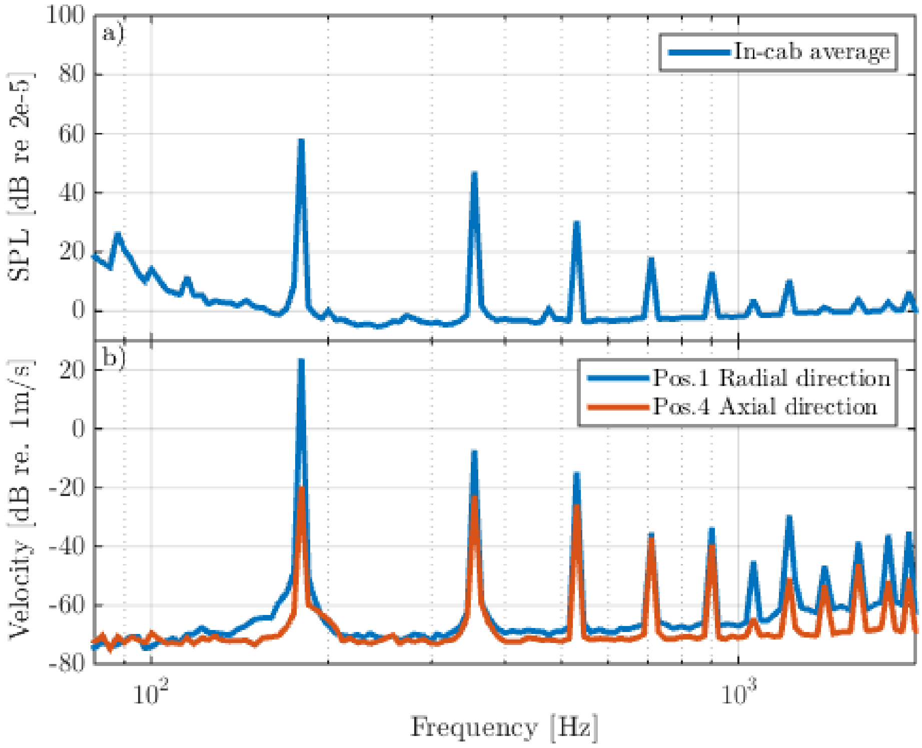

Figure 7.11: a) - Sound pressure levels inside the cab. b) - Velocity level. Excitation with 177 Hz sine wave in radial direction.

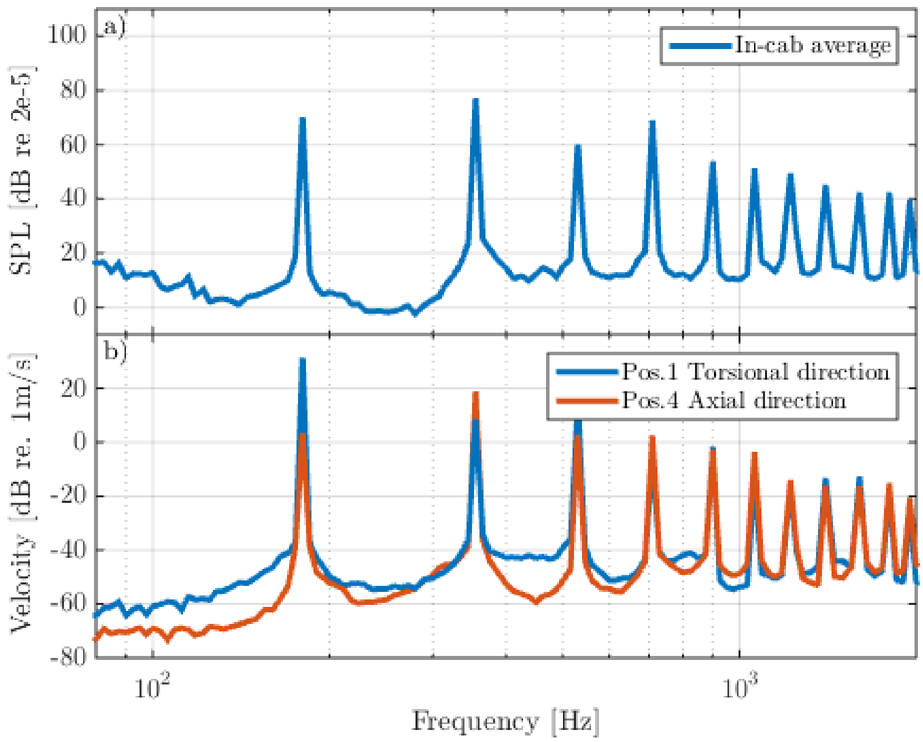

Figure 7.12: a) - Sound pressure levels inside the cab. b) - Velocity level. Excitation with 177 Hz sine wave in torsional direction.

Previous influence of non-linearity in the system has not been evident in the results as such behaviour is not easily detected with white noise excitation. From Figure 7.12 it is obvious that the torsional motion induce distortion as the background level seem raised in relation to Figure 7.11. The time signal of acceleration and force in position 1 has also been examined. While the wave form of the radial excitation acceleration is very close to an ideal sine, the torsional excitation acceleration seem cut and slightly asymmetrical around 0. Raw data time signals are found in Appendix C. This explains the background amplification and the high number of overtones visible in the response. The correlation to radiated sound is again a better match when considering axial velocity instead of torsional. As observed in Figure 7.13. The system is also extremely sensitive to torque applied to the steering wheel. The excitation signal in a) is a 400 Hz sine wave, when no torque is applied this frequency seem to excite the system in a way that causes heavy distortion as the background level rises substantially. However, when approximately 0.5 Nm is applied very little distortion is detected. A 500 Hz sine excitation as is the case in b), yields the opposite relationship.

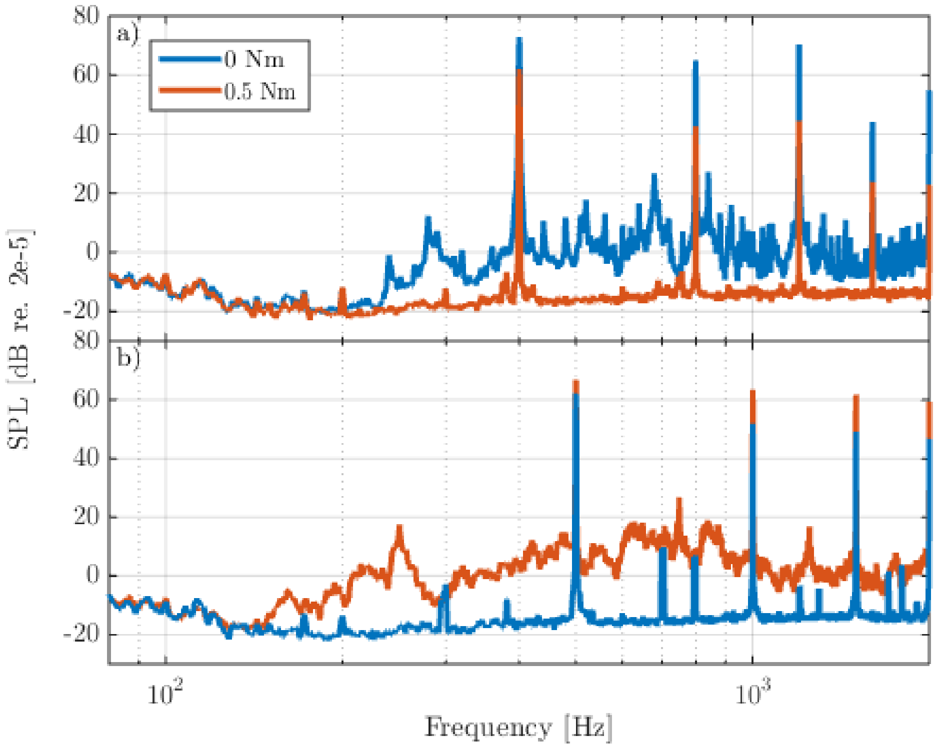

Figure 7.13: Averaged sound pressure levels inside the cab with and without 0.5 Nm torque applied to the steering wheel. Excitation with a) - 400 Hz sine and b) - 500 Hz sine, torsional direction.

The non-linearity is caused by play in the telescope bearing. The sound radiation seem to depend on motion in axial and radial direction rather than torsional, which on the other hand is a key factor for the rattle itself. With the shaft's upper end disconnected, torsional velocity is around 30 dB higher with torsional excitation than radial. Both configurations however, produce similar noise levels, with similar axial and radial velocity.

During normal operation there is of course no way of steering the truck without applying torque to the steering wheel. The torque across the telescope bearing will vary over time as the driver turns the wheel, thus moving the bearing resonance and the influence of the non-linearity in frequency.

The driver will not only influence the system by introducing forces, but also the damping. Driver introduced damping can be observed in Figure 7.14. The damping is here introduced by holding on to the steering wheel in a ten to two position and with forearms pressed down in a twenty past eight position.

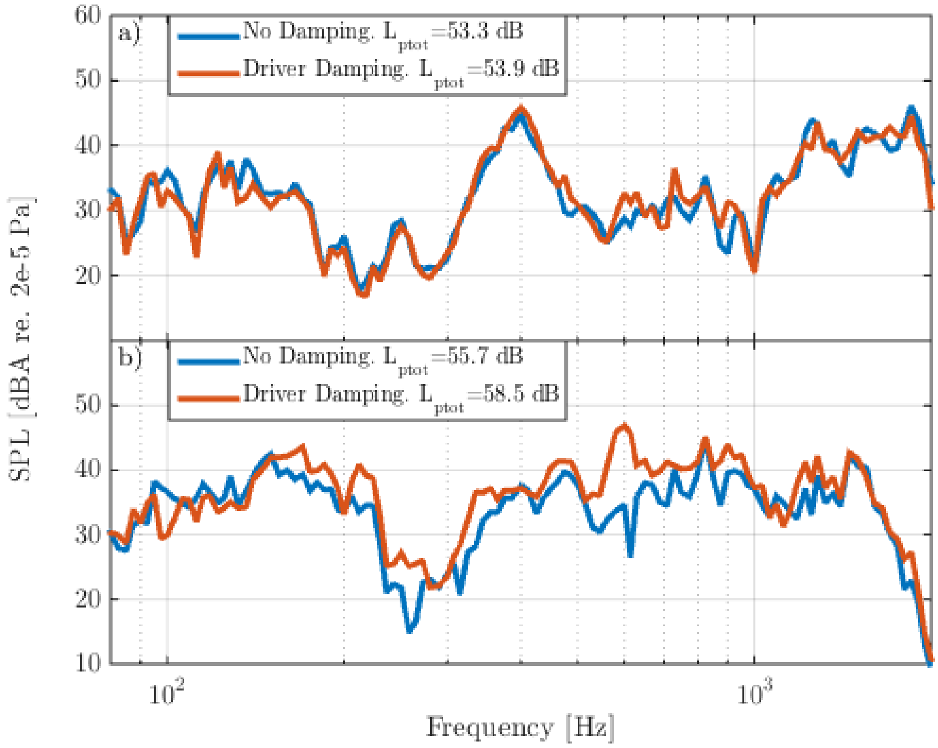

Figure 7.14: Averaged sound pressure levels inside the cab with and without driver introduced damping. Excitation in a) - radial direction and b) - torsional direction.

With radial excitation there is no noticeable difference. In the case with torsional excitation driver damping seem to produce higher levels than without any human interference, this again seems to couple to axial velocity on the upper end of the steering shaft.

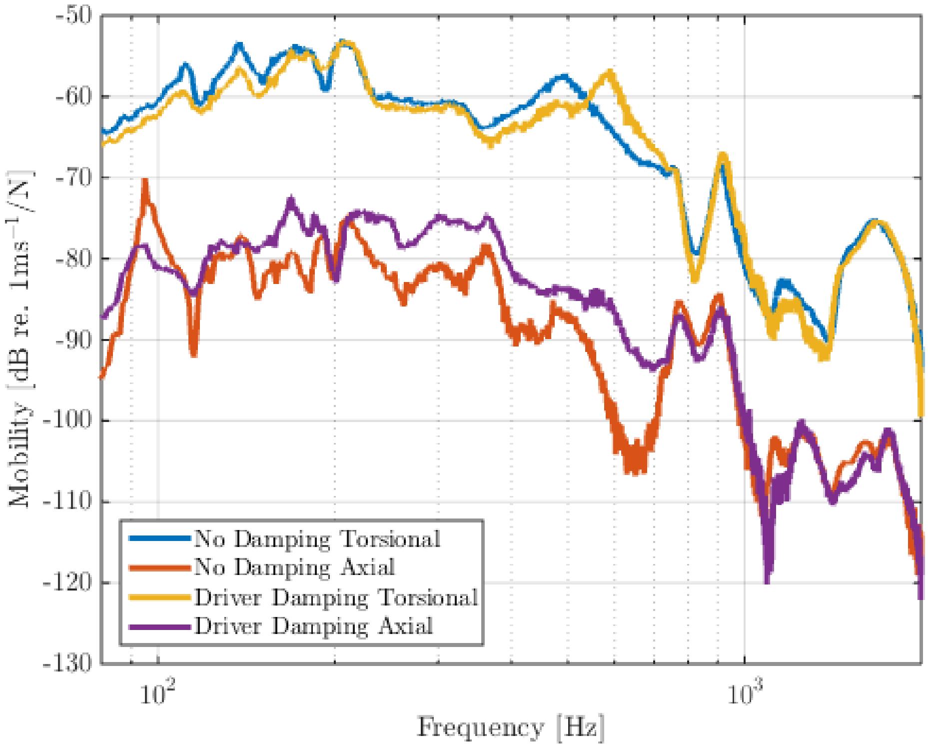

Figure 7.15: Transfer mobility across the steering shaft with and without driver introduced damping.

These measurements effectively conclude that the steering wheel itself is not an important radiator. The equivalent influence in added mass, damping and shielding of any contributing radiator would show as a reduction in the total level in at least some frequency span.

One of the previously set up case studies involved the clock spring and whether this component could distort the radiated sound. The result of these measurements are presented in Figure 7.16

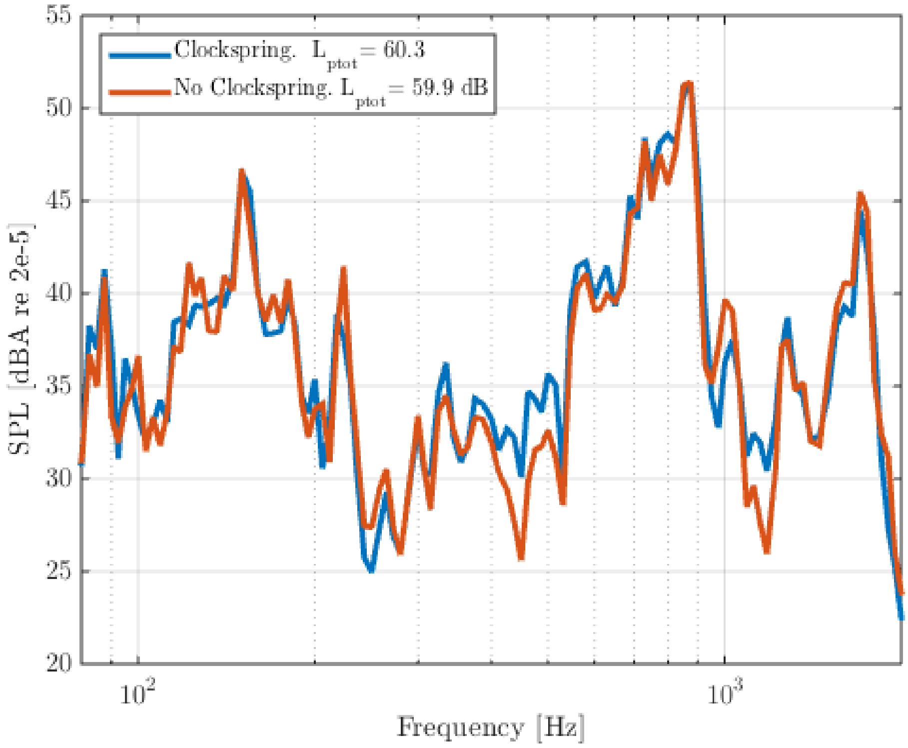

Figure 7.16: Averaged sound pressure level inside the cab with and without clock spring. Excitation in torsional direction.

Under the fact that the steering wheel had to be removed and remounted in order to remove the clock spring, the deviation is below the limit of uncertainty. After a closer inspection of the clock spring it seems unlikely that the poor structural integrity and low mass of the component, compared to the rest of the system, would be enough to change the vibrational characteristics of the system in any significant way. The clock spring itself could of course radiate sound by rattling.

The upper mount between the steering column and the firewall is decoupled by rubber bushings. The lower mount however is a sheet metal bracket with no vibrational decoupling. To investigate the bracket's impact on the frequency response a measurement was made where the bracket was removed. The result is displayed in Figure 7.17. A repeatability measurement is also included. This was carried out two days earlier and both shaker and steering shaft had been dismounted and remounted. The steering wheel is in upright position but moved around since the repeatability measurement. Excitation is in torsional direction.

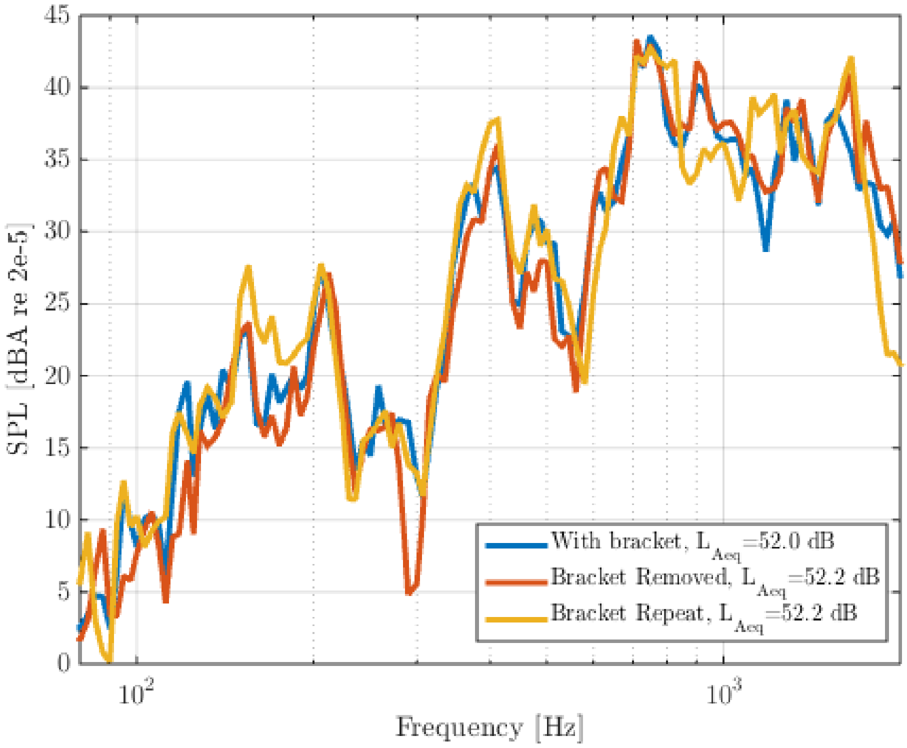

Figure 7.17: Averaged sound pressure levels inside the cab with and without lower bracket. Excitation in torsional direction.

Figure 7.18 shows repeatability with torsional excitation in driving position. The position of column and neck tilt has been changed and reset to position between measurements. The repeatability in radiated noise is considered fair but not as good as the input mobility.

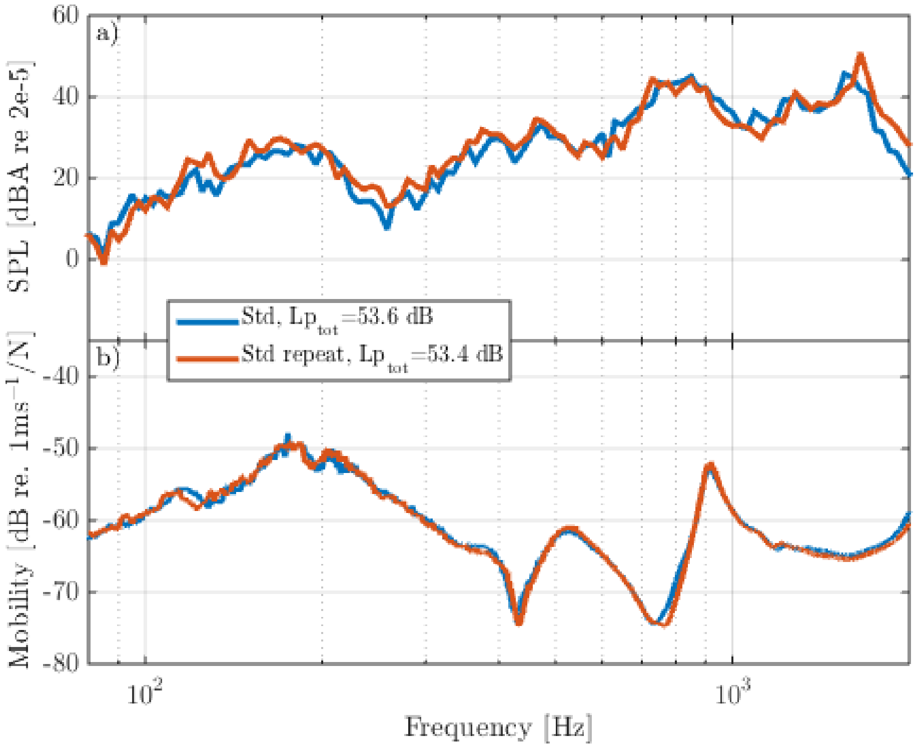

Figure 7.18: a) - Averaged sound pressure level inside the cab. b) - Input Mobility. Steering wheel in driving position and excitation in torsional direction.

7.5 Testing of experimental abatement measures

The in-vehicle measurements were rounded off by testing a few ideas that developed during previous measurements. The measures taken should be considered as evaluation of conceptual ideas rather than proposals for design changes and is observed in Figure 7.19.

The curve 'Std bp' is short for boot padding and refers to the boot between cab floor and steering shaft being padded or rather filled with glass wool. 'Std bp+sb' same 'Std bp' but with the addition of a sand bag folded around the steering shaft supported by the cab floor. The sand bag is of the type used as additional wheight with microphone stands. Finally the 'Std boot up' refers to the boot being mounted facing into the cab covering the cylinder part and instead sealing around the piston.

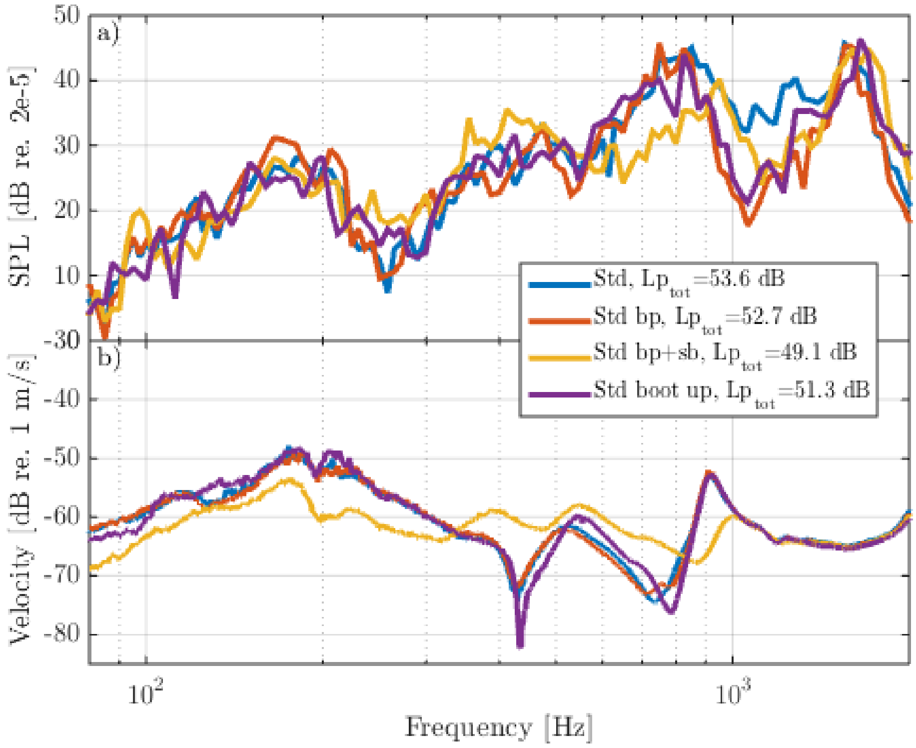

Figure 7.19: a) Averaged sound pressure levels inside the cab and b) input mobility with various treatments. Excitation in tangential direction.

The reduction in total level peaks at 4.5 dB with the sandbag wrapped around the shaft. The added damping is also very clear in the input mobility. Little reduction is however achieved below 600 Hz in any of the cases. The boot padding and boot upwards produce similar result, this points toward that the gain in both cases associates with the increased mechanical coupling to the boot.

Figure 7.20 show the typical spread in sound pressure level between the in cab positions used. A difference in the 10 dB range in the extremes is not uncommon. This shows that in order to comment upon the spectral weighting and vibration to noise relation in a measurement a single microphone position is insufficient for full accuracy.

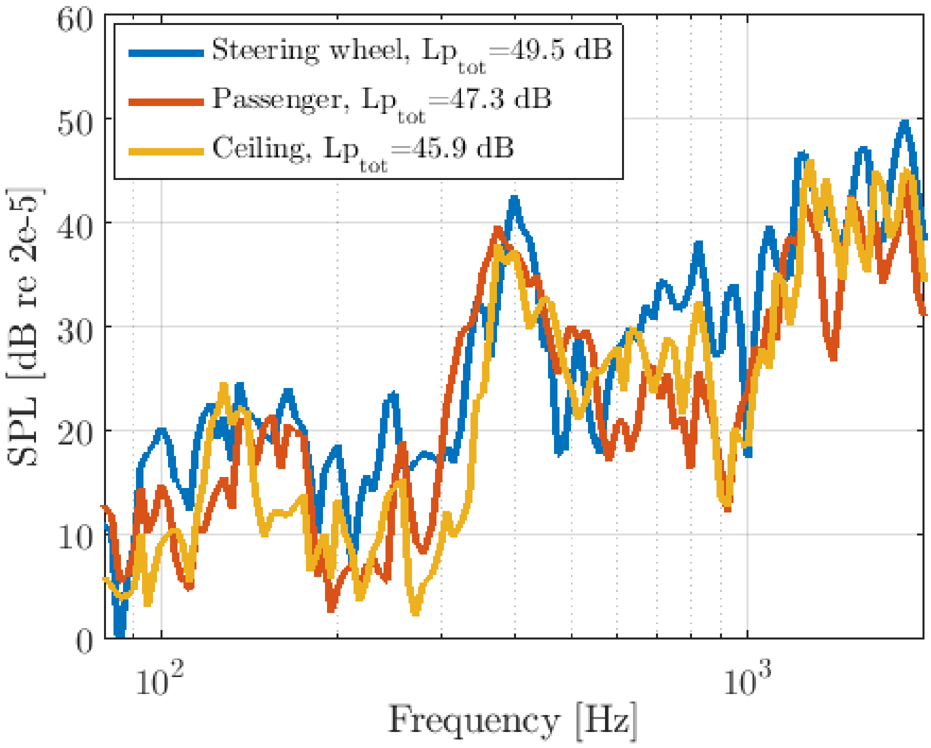

Figure 7.20: Typical sound pressure level spread for the three microphone positions used inside the cab.

Chapter 8

Discussion

Previous work on the steering installation by Kaj Bodlund has led to some conclusions on how the system behaves, but many questions remains unanswered. The work performed during this thesis covers only parts of the full system but has shed light on some of the unknowns. It is obvious that the steering shaft will influence the transfer path in general and the pump whining noise in particular with its own vibrational behaviour. The signs of modal behaviour appears as low as 240 Hz with the first bending wave mode of the steering shaft piston. Measurements also conclude that the shaft can not be considered rigid in torsional direction, something that was previously a parameter of uncertainty.[1, p. 24] Even axial response must be considered, as the universal joints produce substantial resonances in all directions studied. Since P1, P2 and P3 depend on engine rpm, it is difficult to say in general if and to what extent the shaft response coincide with the noise components in a way that amplifies or attenuates the noise. The system does however seem to amplify P2, the spectra around 400 Hz, in comparison to P3 around 600 Hz, assuming an idling engine. Introducing additional damping to the system could even out this phenomenon but will not totally remove the pump whining noise.

The prototype shafts behave differently than the standard shaft but there has been no suggestion of improvement in radiated noise level in general. If anything, the standard shaft seem to perform best out of the selection. The case left out, radial excitation with the 834g shaft, did not show promising results in the isolated setup. The slight improvement in noise level found in [1] connected to the two prototypes cannot be confirmed.

The design also makes the shaft sensitive to static radial forces and bending as this will increase the axial friction. An increase in axial velocity transfer is also clearly visible in the case with introduced driver damping. This is believed to be due to the increased torsional forces in the telescope bearing. The static rotational play of this bearing has not been measured, but it is too small to detect without special equipment. Whether it is the static play alone that causes sound or if the play is further increased by dynamic forces has not been determined. If the cylinder is flexing from round to oval, thus increasing the play during parts of the period, the stiffness could be improved by adding additional rows of balls to the bearing. With the present design the axial vibrational decoupling between cylinder and piston is low. As found during the isolated setup analysis pure axial vibrations are effectively isolated in the bearing above 100 Hz. High torsional or radial velocities on the other hand seem to heavily impair this decoupling and result in higher axial transfer velocities than a pure axial excitation. A similar phenomenon is believed to appear when driving as excitation forces will then act in several directions as a sum of steering pump, engine and road induced vibrations. Since the correlation between axial velocity and radiated noise seem rather good, the design of the axial bearing is crucial not only in terms of pump whining noise but to the influence of the transfer path in general.

When studying non-linearities, a pure sine wave was used as excitation signal. This is convenient but is probably in poor resemblance with the true hydraulic excitation. The presence of overtones corresponding to P2 and P3 is evident even with this ideal sine excitation and concludes that even a P1 sine excitation force at 177 Hz will produce a response containing overtones as P2, P3, both structure borne and airborne. This relates directly to the question at issue in [1, p. 24]. The exact output waveform produced by a hydraulic vane pump depend on a number of factors such as number of vanes and the shape of the inlet and outlet ports. The source characteristics should be further investigated in terms of frequency spectra and pulsation amplitude from both pump and steering gear. As the cab suspension is a significant noise transfer path in the region of the steering pump fundamental < 200 Hz, the only probable solution to entirely eliminate the whining noise is by lowering the source strength. This is achieved by lowering the pressure pulsation from the pump directly or by abatement measures to the hydraulic connection line.

Chapter 9

Conclusions

This chapter contains results from the measurements and the conclusions drawn from these. It also contains the recommendations passed on to Volvo GTT for further research in the future.

9.1 Conclusions

The steering shaft does influence the transfer path to some extent by its resonant nature but the whining noise can not be eliminated simply by flattening its response. Tuned resonators similar to the treatment on the 834g shaft could help lessen the impact targeting a specific engine speed, but would most likely create new problems. Measurements has shown that the cab suspension is a contributing transfer path below some 200 Hz and therefore can not be neglected. This makes it hard to achieve improvements on the first pump order, P1, only by targeting the steering shaft. Investigations have shown that the steering wheel, and the clock spring it contains is not an important radiator. Measurements with the steering shaft decoupled from the steering column point towards that the shaft itself is one of the main radiators, especially in the 450 Hz region.

Vibration measurements conclude that the axial and radial velocities on top of the shafts correlate well with noise from 150 Hz and up. The total velocity level on the shaft is not representative for the in-cab noise radiation and should not be used as vibration reference for in-cab noise measurements. The different shaft prototypes show no major differences between them and it is recommended to take suppressive actions closer to the source i.e. the hydraulic servo pump. Promising results has been obtained from previous work with the hydraulic power lines and shows that a lowering of the source level will produce a corresponding lowering in noise level also in the lower frequency region where transfer paths other than the steering shaft are dominant.

The standard shaft was excited by 400 Hz and 500 Hz sine waves and showed high sensitivity to applied torque. At 400 Hz distortion was created by applying torque whereas at 500 Hz the case was the opposite. This is suspected to be coupled to a non-linearity in the telescope bearing in the steering shaft. It is believed that this bearing design leaves room for further improvement.

References

[1] K. Bodlund, ER-653023, Engineering report, Volvo GTT (2014).

[2] K. Bodlund, ER-623770, Engineering report, Volvo GTT.

[3] K. Ahlin, A. Brandt, Experimental Modal Analysis in Practice, Saven EduTech AB.

[4] Müller BBM, MKII hardware catalog.
URL http://www.pakbymbbm.com/home9610zix/wp-content/uploads/2014/01/PAK_MKII_HB1308_621.pdf

[5] PCB Piezotronics, Model 339A31 Triaxial ICP Accelerometer Installation and Operating Manual.

[6] Brüel & Kjær, PM Vibration Exciter Type 4809 Instruction Manual (December 1977).

Bibliography

Books

1. *Basic Vehicle Technology, Trucks.* (1991). Volvo Truck Parts Corporation, Göteborg, Sweden

2. *Basic Vehicle Technology, Trucks, part 2.* (1995). Volvo Truck Parts Corporation, Göteborg, Sweden

3. *Basic Vehicle Technology, Trucks, part 3.* (1999). Volvo Parts AB, Göteborg, Sweden

4. D.J. Ewins (1995): *Modal Testing: Theory and Practice.* Research Studies Press Ltd., Somerset, England.

Appendix A

List of equipment

Table A.1: Additional Equipment Data

Brand	Model	Serial number
PCB Piezotronics	339A31	6603
		6599
		6518
		6215
Brüel & Kjær	4507 B004	2154333
		2154332
		2154331
Brüel & Kjær	4508 B	2251374
		2251363
		2251361
		2251360
Brüel & Kjær	8230-001	54931
Goodman	Type 790A	552

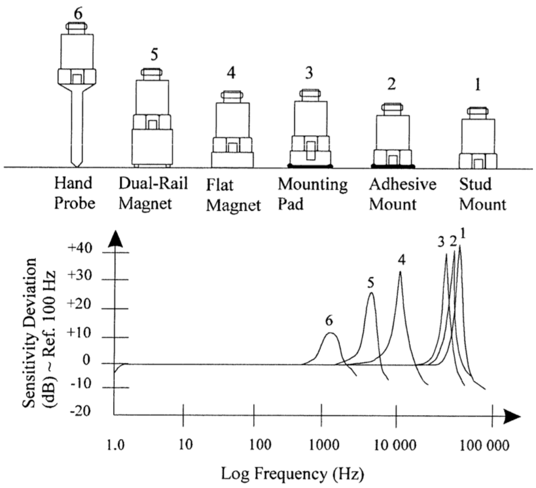

Figure A.1: Assorted mounting configurations and their high frequency effects.

Appendix B

Vehicle Configuration

Table B.1: Vehicle Configuration Sheet

Administration
6 Wheels thereof 4 driving
60.0 tonnes, gross combination weight
13 L. Engine
Front axle load 9.0 tonnes
21 tonnes, rear axle load
Left hand side steering
XM = 7940mm, rear axle pos.
Chassis height high
Engine with mounting and equipment
Without left side liquid fuel tank
550 litre, right side fuel tank
Exhause direction, left
Ad-Blue tank usable volume 90 litres
Wheel, Suspension and Steering

High ground clearance-low offset
2 axle, 2 driven, air suspension
Without pusher axle capacity, first
Without trailing axle capacity, first

Frame springs damping wheel

Rear frame lenght, 3345mm
Leaf spring suspension
Parabolic spring (normal stiffness) front
Air spring, rear
Tire 385/65, front axle
Tire 315/80, drive axle
Without trailing axle tire
Without pusher axle tire

Body, Cab and Interior

High sleeper cab
Front cab suspension mechanical spring

Appendix C

Additional Plots and Data

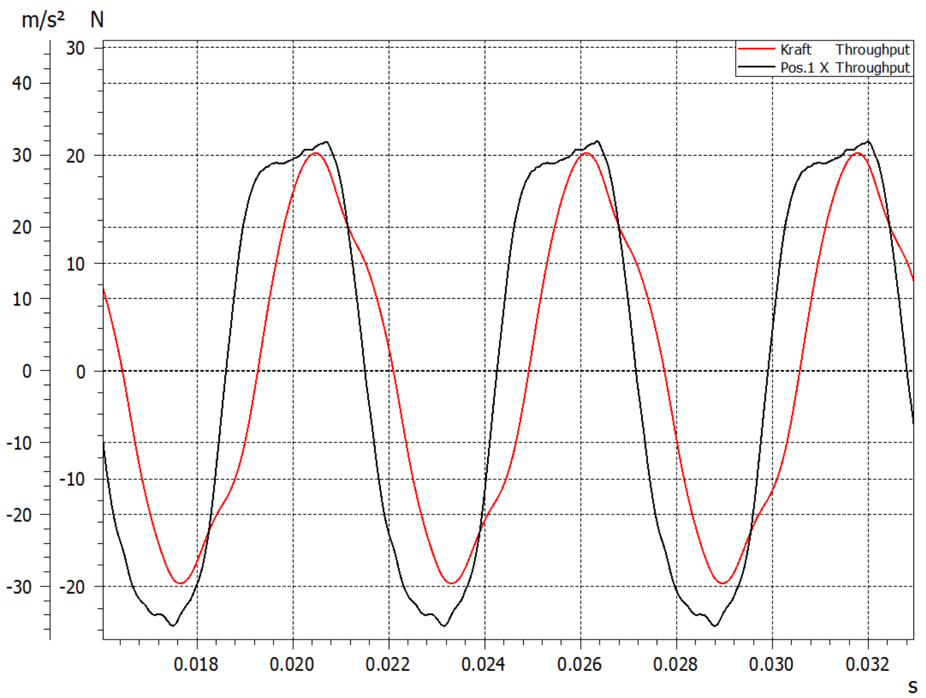

Figure C.1: Time signal of force and torsional velocity at pos 1. Excitation 177 Hz sine in torsional direction.

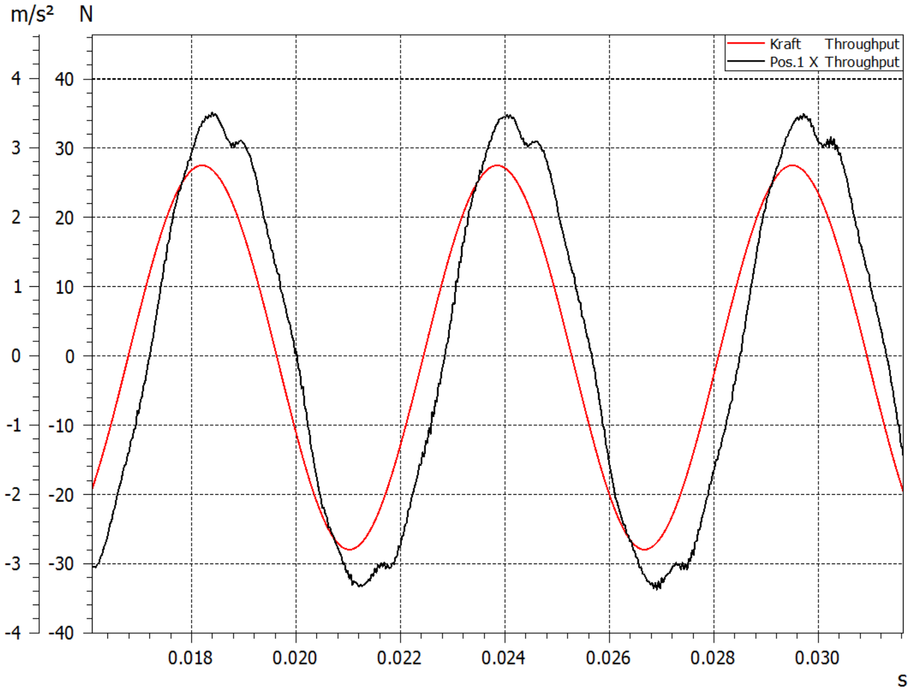

Figure C.2: Time signal of force and radial velocity at pos 1. Excitation signal 177 Hz sine in radial direction.

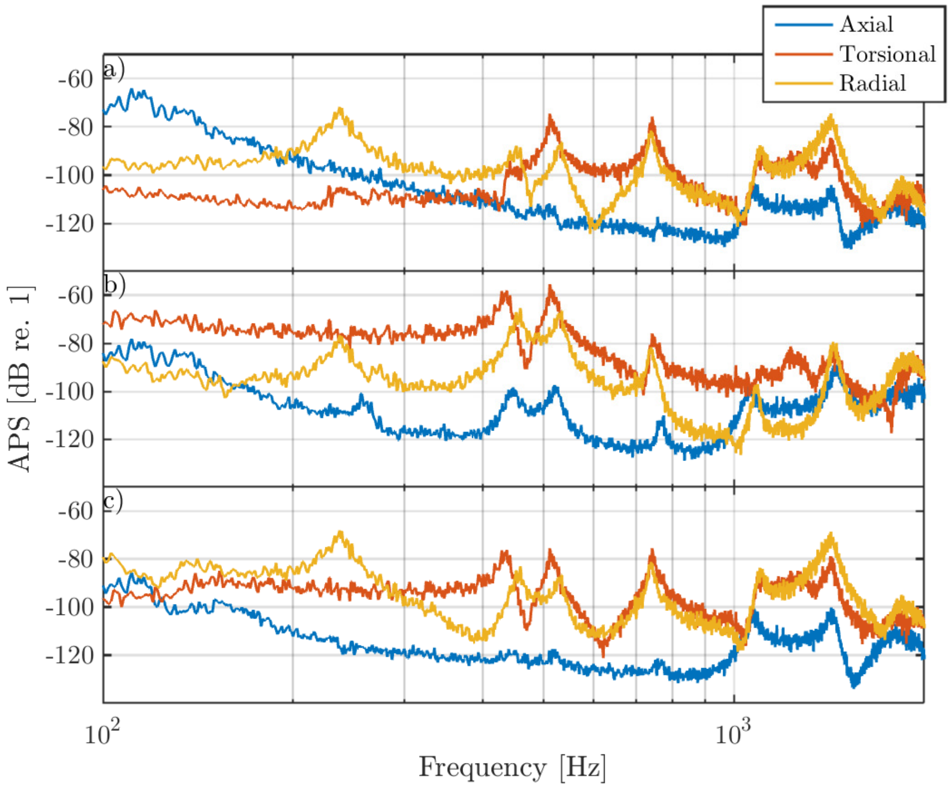

Figure C.3: Comparison of velocities in Position 4 when exciting in different directions. a) - axial velocity, b) - torsional velocity and c) - radial velocity.

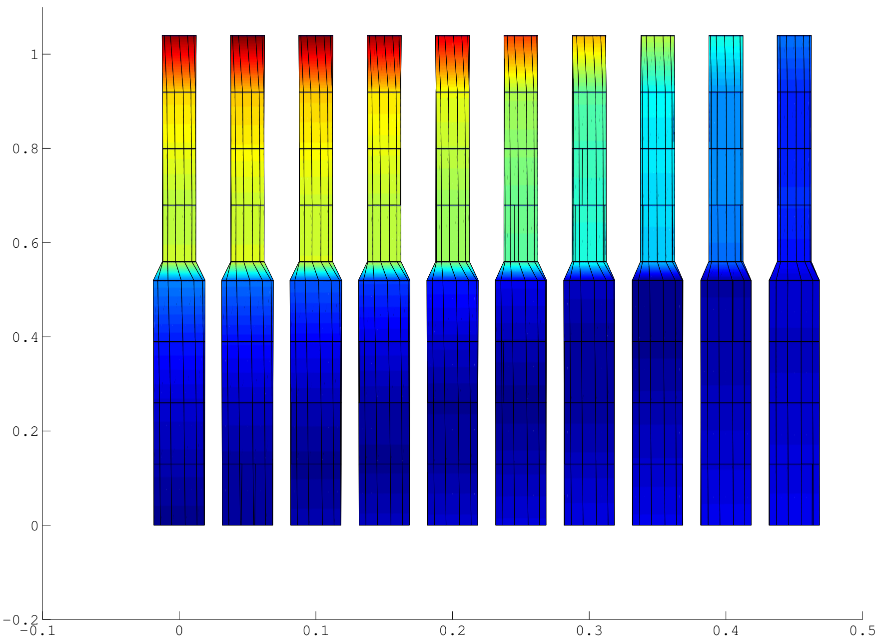

Figure C.4: Torsional motion of fully extended standard shaft at 415 Hz. Excitation torsional, shaft freely suspended.

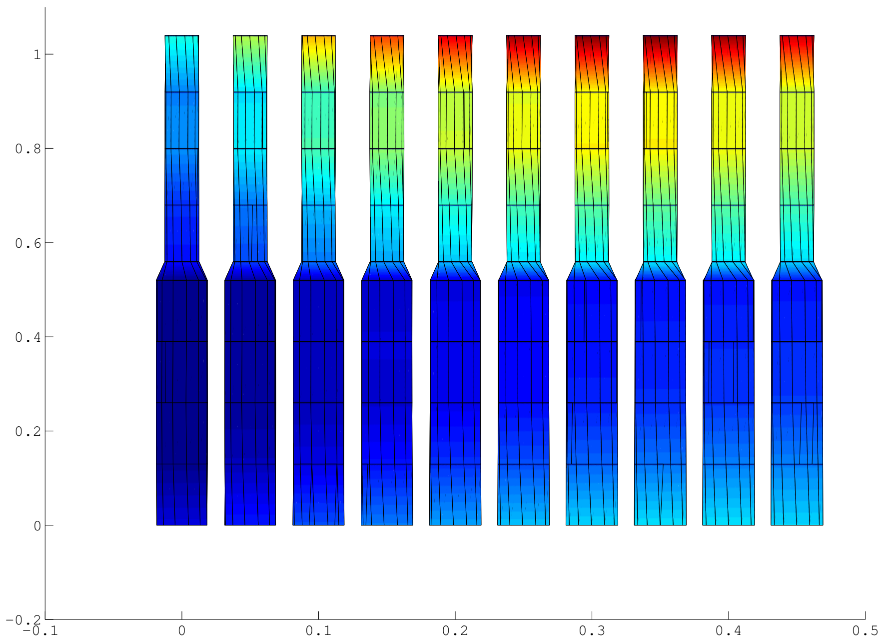

Figure C.5: Torsional motion of fully extended standard shaft at 490 Hz. Excitation torsional, shaft freely suspended.

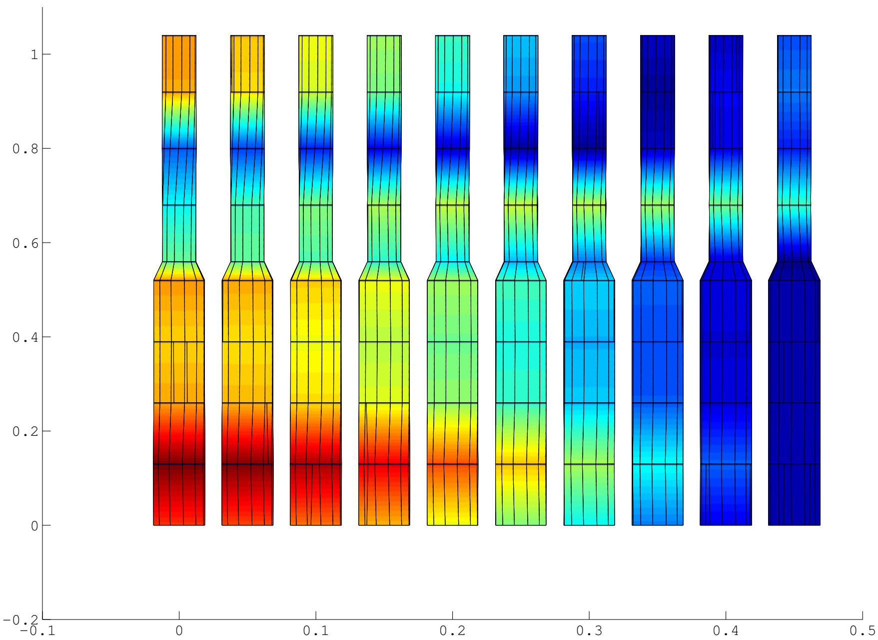

Figure C.6: Torsional motion of fully extended standard shaft at 760 Hz. Excitation torsional, shaft freely suspended.

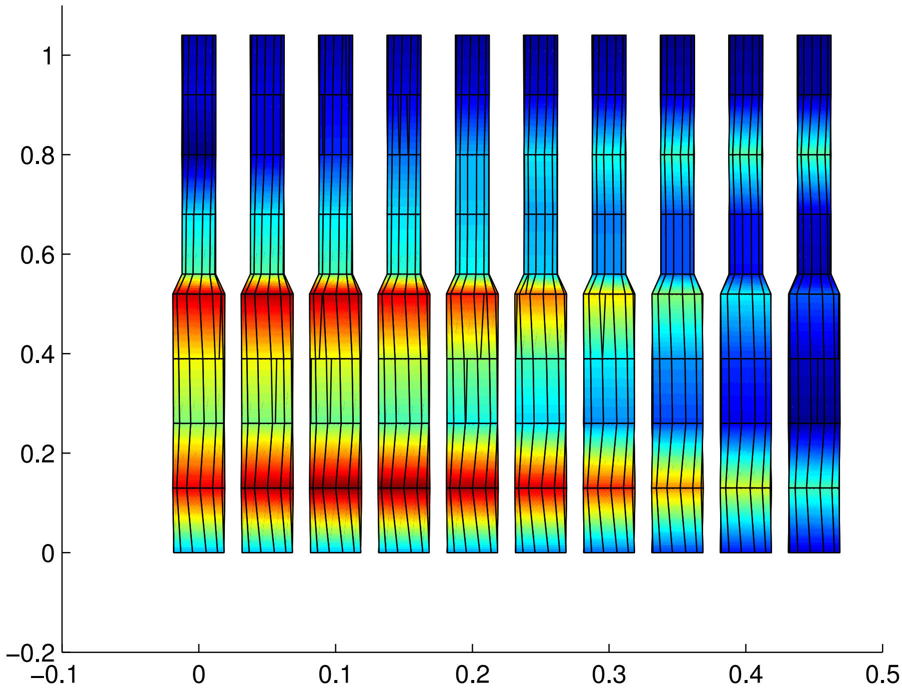

Figure C.7: Torsional motion of fully extended standard shaft at 1200 Hz. Excitation torsional, shaft freely suspended.

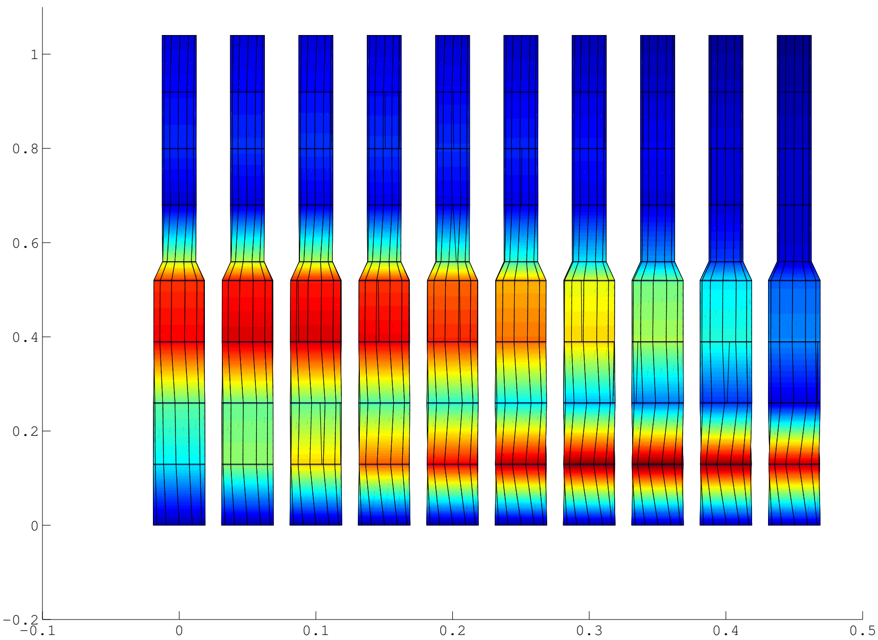

Figure C.8: Torsional motion of fully extended standard shaft at 1340 Hz. Excitation torsional, shaft freely suspended.

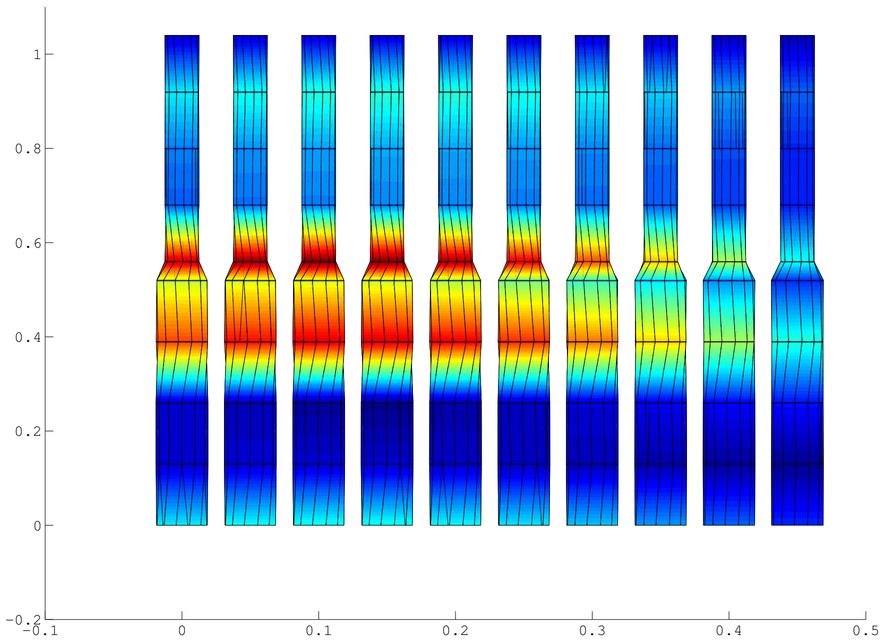

Figure C.9: Torsional motion of fully extended standard shaft at 1640 Hz. Excitation torsional, shaft freely suspended.

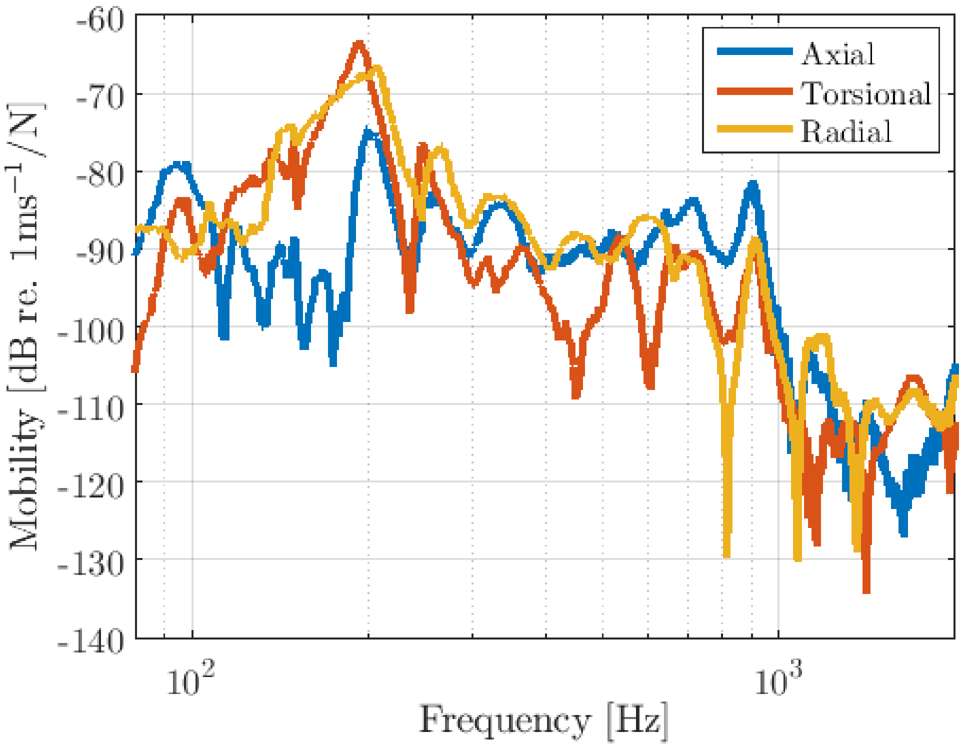

Figure C.10: Transfer mobility to pos. 6, just below the steering wheel. Excitation in tangential direction, steering wheel position upright.

Figure C.11: The truck used for all the in-vehicle measurements.